International Journal of Machine Tools & Manufacture 160 (2021) 103653

Contents lists available at ScienceDirect

International Journal of Machine Tools and Manufacture

journal homepage: http://www.elsevier.com/locate/ijmactool

Analytical springback assessment in flexible stretch bending of complex shapes

J. Ma *, T. Welo **

Department of Mechanical and Industrial Engineering, Norwegian University of Science and Technology (NTNU), Trondheim, 7491, Norway

ARTICLE INFO

Keywords:
Springback
Flexible stretch bending
Analytical solution
Full moment
Profile

ABSTRACT

Stretch bending is commonly used in the fabrication of profile-based shapes. However, one of the challenges in many bending-type forming processes is controlling springback upon unloading. Springback appears sensitive to upstream and in-process parameters, making prediction and control difficult. The springback problem is particularly important in forming processes where stringent control strategies are needed to assure product dimension, process flexibility and overall equipment effectiveness. In this research, we present an analytical framework for springback assessment in a stretching-controlled bending process. A new, flexible rotary stretch bending machine is designed and built, which allows the manufacture of complex-shape profiles with varying curvatures, including straight portions, with low tool investments. Furthermore, a Full Moment (FM) analytical model is developed for springback assessment. The modeling strategy employs a full moment distribution along the entire profile upon bending, introducing a stretching-controlled moment transition between different curvature portions such that the springback contribution from the plastic moment outside the theoretically bent portions is considered. Additionally, the influential factors related to material, geometry and process, including the applied stretching strains, are comprehensively considered. In this way, the modeling strategy enables accurate evaluation of springback in the flexible stretch bending process. Moreover, the proposed forming process is validated by a series of experiments conducted for a wide range of stretching levels using rectangular hollow aluminum alloy profiles. This forming strategy demonstrates high capability for controlling springback and dimensional accuracy. By comparing experiments, numerical simulations and analytical calculations, this proves that the developed FM model provides accurate and efficient assessment of springback. The average relative error provided by the FM model is 2.2%, as compared to 10.5% for a classical method used for comparison. Using the analytical model combined with numerical simulation, the crucial deformation characteristics, including stretching-dependent evolution of strain transition, are revealed. Overall, the FM analytical strategy has proven its capability as an effective tool, which can make springback knowledge more explicit, generic and reuseable for stretching-controlled bending processes.

1. Introduction

In response to the more stringent regulatory requirements on energy consumption and CO_2 emission, weight reduction has become an important concern in the automobile industry [1,2]. Profile-like lightweight products and product families are attracting more and more attention to achieve the new requirements [3,4]. Up to now, multiple forming technologies have been developed to manufacture profile-based components and semi-finished parts. Among these methods, bending as well as bending-based technologies are among the most commonly used ones in several application areas [5].

During the past decades, a series of methods have been developed to fabricate bent shapes; examples are given as stretch bending [6], rotary draw bending (RDB) [7], roll bending [8], torque superposed spatial bending (TSSB) [9], extrusion bending [10,11], free form bending [12], and recently-reported hydro-forging bending [13]. In all these bending processes, however, springback is one of most significant issues that seriously affects the dimensional accuracy of the formed product, the process flexibility, the manufacturing cost, and the overall equipment effectiveness (OEE) [14–17]. As springback appears sensitive to

* Corresponding author.
** Corresponding author.
E-mail addresses: jun.ma@ntnu.no (J. Ma), torgeir.welo@ntnu.no (T. Welo).

https://doi.org/10.1016/j.ijmachtools.2020.103653
Received 21 September 2020; Received in revised form 13 November 2020; Accepted 15 November 2020
Available online 19 November 2020

in-process and process parameters throughout the manufacturing chain [18], effective prediction and control of springback are facing considerable challenges.

Stretch bending, owning to its high dimensional accuracy and reproducibility, is a widely used process for high-volume production of bent shapes [3]. From the perspective of kinematics, conventional stretch bending can be divided into two categories; i.e., stress (or force)-controlled processes and strain (or kinematically)-controlled processes [5,19]. The former often includes open-arm and rotation-arm type processes, as shown in Fig. 1 (a) and (b), which are usually used for forming symmetric parts. The latter usually includes single-rotation and double-rotation type movements, as shown in Fig. 1 (c) and (d), which are widely used for forming more complex shapes. However, a challenge faced by conventional stretch bending is low flexibility, high tool cost and high machine or press cost. In most cases, one set of tools can only support one product configuration, making it difficult to meet today's demand for mass customization at low cost [6]. As a countermeasure, some attempts have been made to improve the flexibility in stretch bending. One example is using multi-point dies to replace the conventional dies based on the above-described stretch bending methods [20,21]. This multi-point flexible tool strategy is also used for forming complex-curvature sheet parts with reduced part specific tool cost [22]. For this method, however, the dimensional accuracy and surface quality of the formed parts are much lower than those of conventional stretch bending due to the discontinuous surface topology of multi-point dies. Recently, a new concept for flexible rotary stretch bending was introduced for fabrication of complex three-dimensional (3D) profiles [6]. In this strategy, enhanced flexibility is realized by adding rotational axes combined with a tooling concept utilizing part-specific inserts, thus enabling the manufacture of multiple part configurations with lower tool investments. However, the springback problem is more difficult to control as some new characteristics and mechanisms come into play, compared to conventional stretch bending. Therefore, how to effectively assess the springback behavior becomes a more urgent issue which needs to be solved in stretching-controlled flexible bending processes.

To address the springback problem in stretch bending, numerous efforts have been made during the recent decades, using experimental (empirical), analytical as well as finite element (FE) methods. Numerical and analytical methods are commonly used to reduce or replace 'trial-and-error' associated with more expensive physical experiments. FE analysis presents superiority for considering nonlinear material behaviors and complex workpiece-tool contacts in forming analysis [23]. However, FE is time-consuming, and it needs deep modeling knowledge often not present in many small and medium size (SME) manufacturing companies. Analytical approaches, despite their simplifications, offer rapid springback evaluated and the associated mechanisms can be efficiently and qualitatively estimated [24], thus providing an effective means to make process and springback knowledge more explicit and reuseable, which will leverage dimensional control in metal forming.

As starting point for developing advanced analytical models for springback assessment, the fundamental theory of stretch bending and the state-of-the-art of the existing analytical models must be critically reviewed. They are briefly introduced in the following.

1.1. Theory of stretch bending

In stretch bending, the strategy employed for applying combined stretching and bending as well as nominal stretching history is of importance. Stretching can be applied in different sequences; namely, before bending (pre-stretching), during bending (in-process stretching), and after bending (post-stretching) [5,6]. An appropriate strategy for applying stretching can improve the quality of the formed component along with the performance of final product. Too severe stretching, on the other hand, may induce damage to the formed parts, negatively affecting product performance [25]. From the perspective of springback reduction, the total accumulated stretching strain and the loading path can make a significant difference. Here the latter should be applied proportionally to avoid local unloading, especially towards the end of forming prior to unloading. The former determines the stress gradient across the cross-section at the instant of unloading, which mainly determines the magnitude of springback.

The distribution characteristics of stress and strain in stretch bending can be characterized by neutral layer (NL) shifting. As shown in Fig. 2 (a), under the assumption of pure bending without stretching, the NL can shift from the centriod of the section, especially at tight radii, among

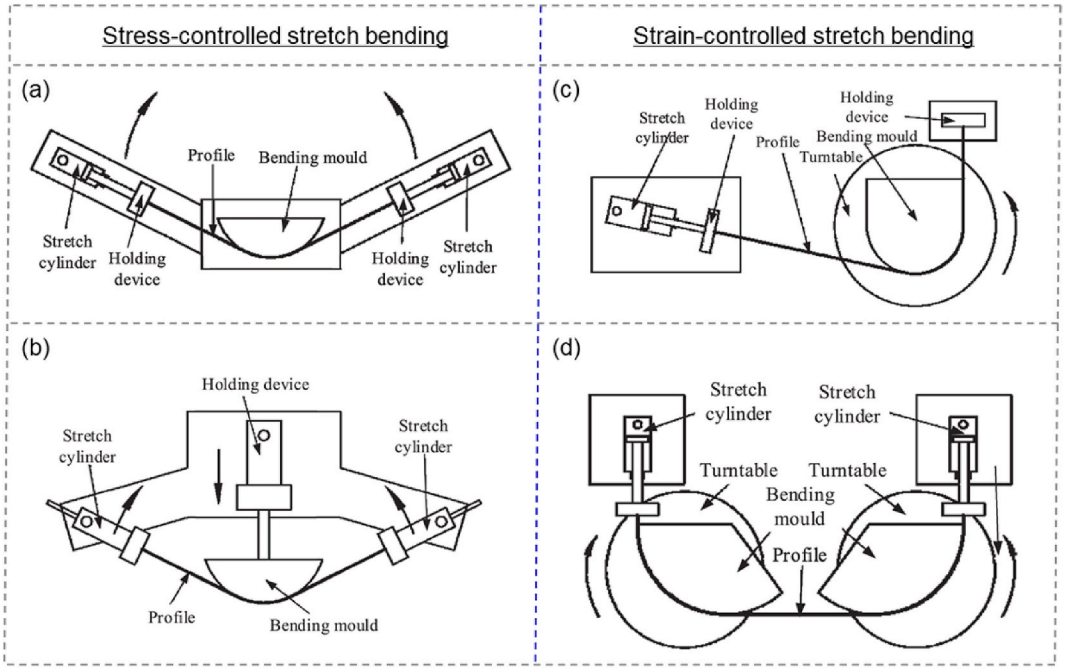

Fig. 1. Schematic view of process principles of stretch bending methods [19]: (a) open-arm type; (b) rotation-arm type; (c) single-rotation type; (d) double-rotation type.

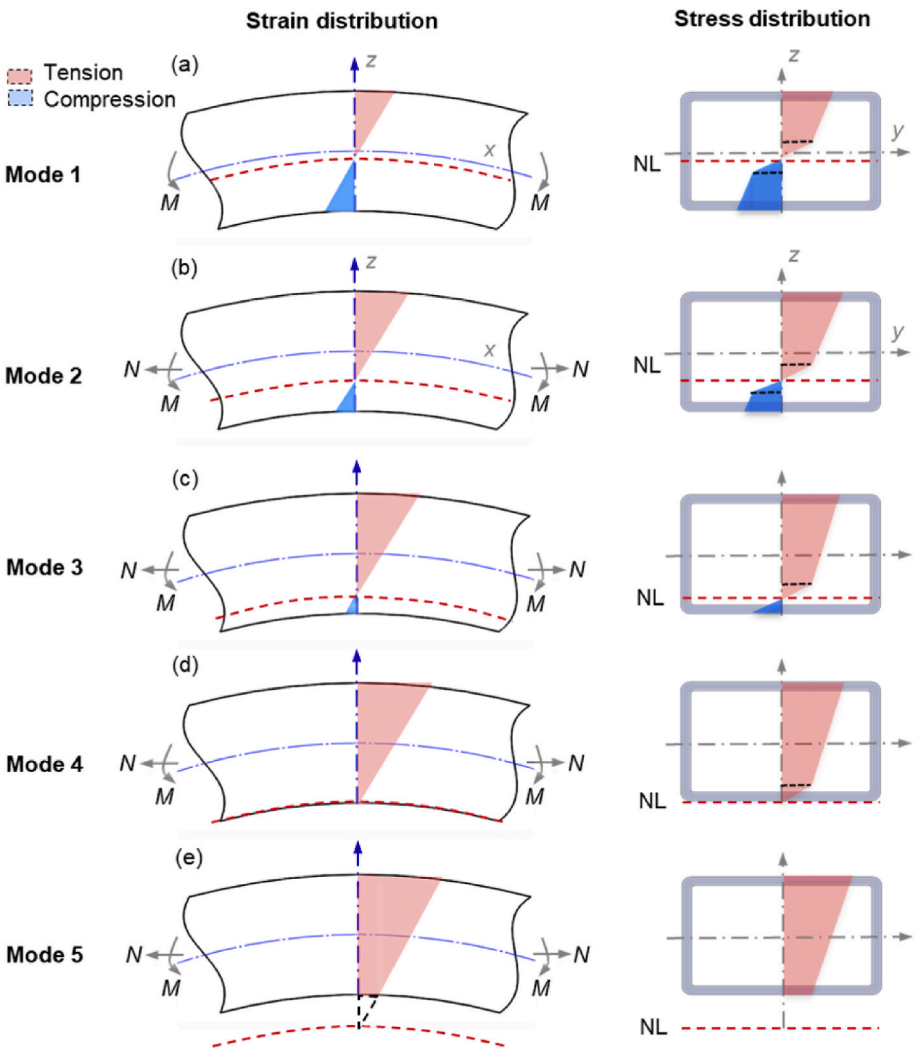

Fig. 2. Stress and strain distribution of stretch bending of profile.

others, due to mass conservation effects induced transition of tension-compression across the depth of the cross-section upon plastic deformation (bending). Both direction and distance of NL shifting depend on the material properties as well as the bending curvature. For most metallic materials, with similar stress-strain behavior in tension and compression, the NL shifts towards the curvature center; however, for some alloys with initial tension-compression asymmetry, such as magnesium alloys, outward shitfing may occur under pure bending [24]. When applying stretching in bending process, the NL moves towards the bending center, as shown in Fig. 2 (b) ~ (d). If the applied stretching strain is sufficiently large, the (theoretical location of) NL can move outside the cross-section, as shown in Fig. 2 (e).

According to the NL position, stretch bending can be categorized in terms of different modes as follows: Mode 2 (Fig. 2 (b)) with both tensile and compressive plastic zones in the cross-section; Mode 3 (Fig. 2 (c)) with a tensile plastic zones and a compressive elastic zone; Mode 4 (Fig. 2 (d)) is a state without a compressive deformation zone; and Mode 5 (Fig. 2 (e)) with the entire cross-section under tension. In this mode, the stress gradient across the depth of the profile is reduced, and the springback is dramatically reduced compared to pure bending. Mode 5 is usually used in industrial practice [5]. Thus, Mode 5 bending will also be focused herein, seeking to develop an advanced analytical model for accurately assessing springback in the flexible rotary stretch bending process to be presented in the continuation.

1.2. *Review of existing analytical models*

At present, extensive analytical models have been developed to analyze springback problems in bending-type processes. To name a few, Yu and Johnson [26] analytically studied the springback of a beam under pure bending subjected to an external axial force, showing that the axial force can effectively reduce springback. However, this work employs a simple perfect-plasticity material model without considering working hardening, which can only be used for a very rough analysis of beam bending cases. Geiger and Sprenger [27] proposed an analytical model of springback for stretch bending of rectangular extrusions based on element bending theory, in which the geometrical and mechanical parameters are considered for springback analysis. In this method, however, the changes of geometrical dimensions, like thinning is not included, reducing the accuracy especially for bending cases under high stretching. In addition to springback, similar methods were also used to analyze forming loads and bendability in stretch-bending within fully elastic, primary-plastic, and secondary-plastic regimes in Refs. [28–30]. Based on element bending theory, Zhao et al. [31,32] and Zhai et al. [19] conducted analytical modeling for springback under small-curvature sheet bending, and extending it to modeling springback of profiles in pre-bending-tension process. For the above-mentioned models, the stress distribution of the entire cross-section is considered for prediction of the (elastic-)plastic moment at the instant of unloading. However, there exist also more simplified formulations, which only take

partial sectional regions into account; for example, Zhu and Stelson [33] proposed a two-flange model for springback in stretch bending of rectangular profile. In this model, only the outer and inner flanges of the rectangular section are used to calculate the bending moment, while the stress distribution across the webs is ignored. Due to the geometrical assumption, however, the application of a two-flange model is only limited to simple symmetric sections. The prediction accuracy becomes more sensitive to sectional dimensions like the thickness of flanges/sidewalls, width and height. In addition to the material and geometrical parameters, Zhu and Stelson [33] and Liu et al. [34] also considered workpiece-tool friction within the above-described analytical frame by introducing a capstan model, thus enabling the modeling of friction effects on springback. However, Miller et al. [35,36] reported that friction can only exert a very slight influence on the forming process—although the part should be lubricated in most cases for best results from post-tension.

Moreover, analytical modeling of springback can provide more than prediction accuracy. Owning to high solution efficiency, analytical methods can be used for real-time, in-process control of bending processes. To name few cases, Geiger and Sprenger [27] used an analytical method together with artificial neural networks (ANN) to optimize process parameters from the relation between a force-displacement chart and springback ratio, and the model is further applied to develop an on-line control circuit. Welo and Granly [37,38] employed an analytical steering model to design a closed-loop-control system of springback in rotary draw bending. Unlike conventional control strategies, this novel control strategy is attractive for high-volume production since the high solution efficiency does not impact cycle time. Grzancic et al. [39] derived an analytical model for predicting wall thickness reduction and forming force for a radial-indentation, incremental profile forming process. It is claimed to provide time-efficient estimation of process output parameters, e.g. forming force, which is of interest for industrial closed-loop control applications. From the abovementioned studies, another attracting point of analytical models can be presented is the design of intelligent systems for controlling springback. However, the capability of springback control still depends highly on the accuracy of the analytical models.

The body of research on analytical springback in bending processes is obviously more extensive than the above-summarized ones and many not mentioned have made great contributions to addressing the problems involving springback. However, many of these studies focus mainly on conventional stretch bending processes, which can only solve the springback problems of constant-curvature geometries. As for more generalized forming processes, as well as emerging processes for fabrication of more complex shapes, there is still a lack of advanced analytical methods applicable for springback analysis. Especially, for the springback in stretching-controlled flexible bending of complex geometries with varying-curvatures configurations, very few relevant studies, if any, do exist.

To make a contribution to fill these identified research gaps, this paper aims to develop an advanced analytical framework for accurate and efficient assessment of springback in a flexible, stretching-controlled bending process. First, a new flexible stretch bending method is proposed, and a full-scale machine system is built, allowing forming of complex-shape profiles with varying curvatures, bend angles, as well as a kinematically-controlled strain history. Furthermore, a novel analytical framework for springback prediction will be developed by considering the full moment distribution along the entire formed profile as well as influential parameters related to material, geometry and process, thus providing an accurate and rapid assessment of springback. Moreover, a series of carefully designed physical experiments and FE simulations will be conducted to validate the process capability of the proposed flexible bending method along with the prediction accuracy of the developed analytical model. Finally, based on analytical model and FE simulation, the deformation characteristic of the new process will be discussed for the better understanding of how these affect the springback behavior.

2. Novel flexible stretch bending method

2.1. Process description

A new stretch bending process is developed to enhance the flexibility of conventional stretch forming, seeking to meet today's rapidly changing demands for complex product geometries. Fig. 3 presents a schematic view of the CAD model of the machine design, which is based on the 3D bending strategy reported in Refs. [6]. By adding multiple rotational axes in conjunction with an innovative design of dies with different geometrically configurations, machine flexibility can thus be improved to accommodate different product geometries.

As shown in Fig. 3, this machine system consists of two opposing sets of bending arms. Each arm provides three degrees of freedom (DOFs), and are described as follows:

- Rotational movement in the vertical *x*-*z* plane controlled by Axis 2 and Axis 3.
- Rotational movement in the horizontal *x*-*y* plane controlled by Axis 4 and Axis 5.
- Translational movement in the base structure (*x*-direction) controlled by Axis 1.

As shown in Fig. 4 (a) and (b), each pair of bending arms provide rotational moments around individual pivot points, continuously stretching the profile while this is clamped and prevented from sliding at the ends. The distance (x) between the individual axes and the perpendicular distance from the individual pivot point to the inside of the profile (y in Fig. 4 (a) and z in Fig. 4 (b), respectively) is crucial for the stretching path of the profile upon forming. If the locations of pivot points do not ensure a continuous increase of the strain of the entire workpiece during the bending stroke, the workpiece may experience local elastic unloading, thus causing large springback upon unloading. In this study, the location of the pivot points for two rotation directions (as shown in Fig. 4 (a) and (b)) are determined based on the above guideline. The translational movement can accommodate profiles with different lengths, geometries and shapes, providing flexibility for various products needed in mass customization. In addition, this degree of freedom provides pre-/post-stretching or in-process (simultaneous) stretching capibility for optimizing the stretching path with regard to springback. For the built machine, Axis 2 and Axis 3 use electric servos and rotary absolute encoders; Axis 4 and Axis 5 are controlled by hydraulic servo actuators and linear absolute encoders; and Axis 1 is realized by the movement of the base platforms relative to each other, controlled by hydraulic servos. As illustrated in Fig. 5, based on the above design principle, a full-scale 3D stretch bending machine is designed, built and installed in the laboratory. This new machine system can produce both two-dimensional (2D) and 3D bending configurations of large profiles with lengths up to more than 2 m, different cross-sections and geometry configurations.

2.2. Springback definition

When the bending arm is rotated to the final stop position, the clamp tools are released and springback occurs instantly during unloading. Springback induces changes of local curvature along the part, making reduction of chord heights in the two bending directions. In this research, however, we consider 2D bending only (activating axes 2 and 3) to fundamentally study the springback behavior of the bending method.

Fig. 6 shows a reference line with the distance (L_r) between points J and K (or between points J' and K') used to define the springback chord height. First, the chord height (H) of the part before springback is defined as PO, representing the distance from the reference line to the

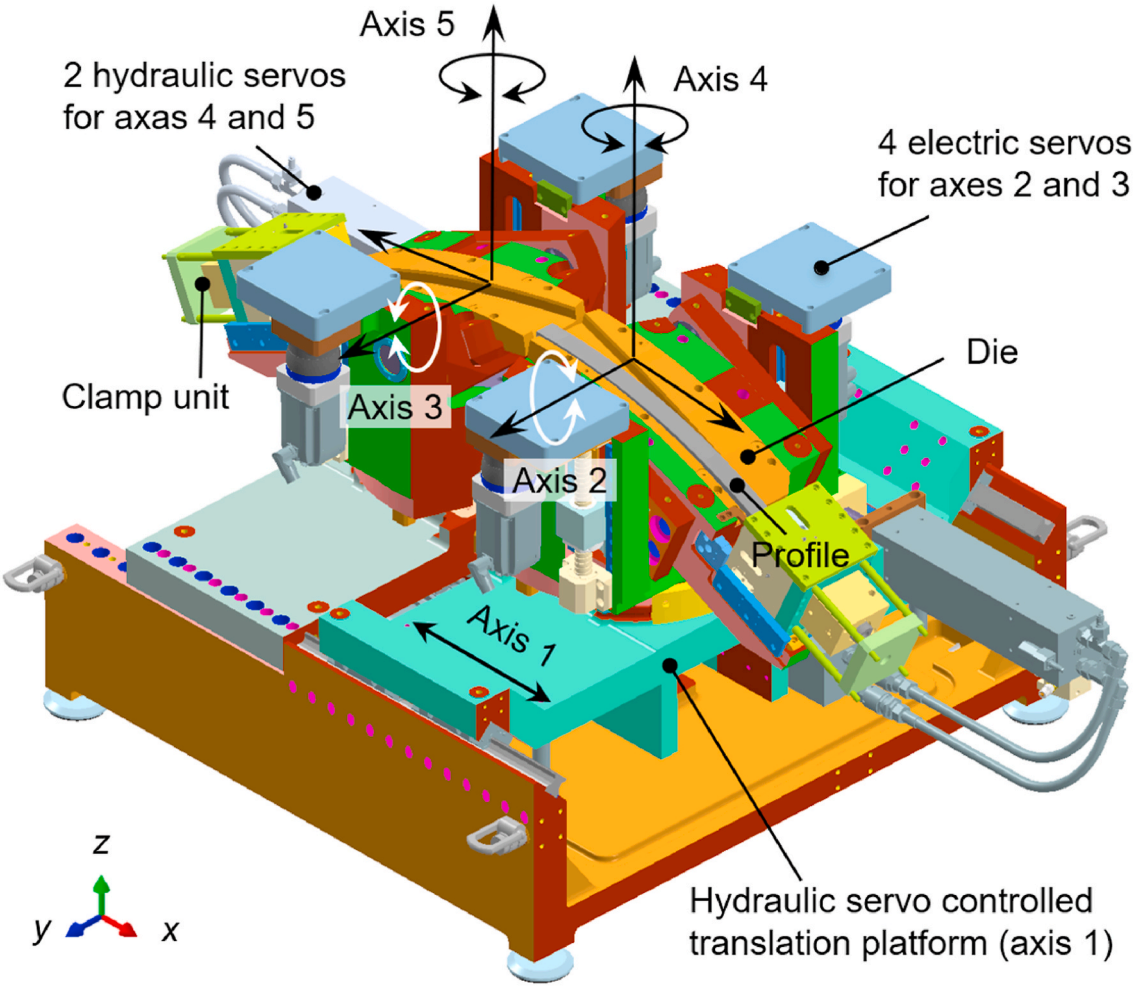

Fig. 3. Novel 3D, flexible rotary stretch bending process.

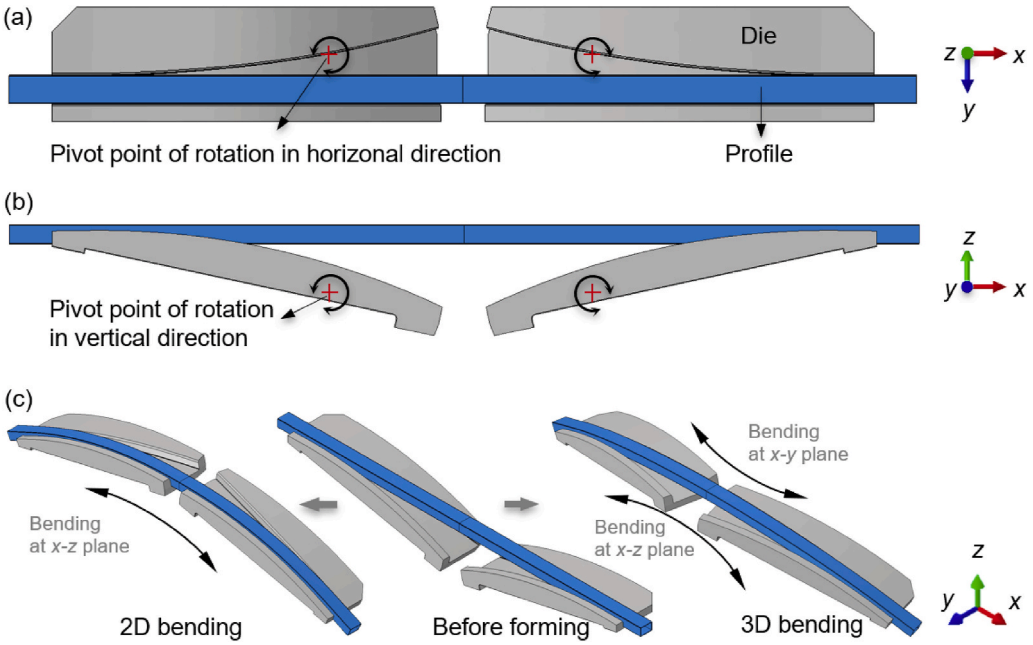

Fig. 4. Geometries of formed parts: (a) top view before forming; (b) side view before forming; (c) schematics of 2D/3D forming processes.

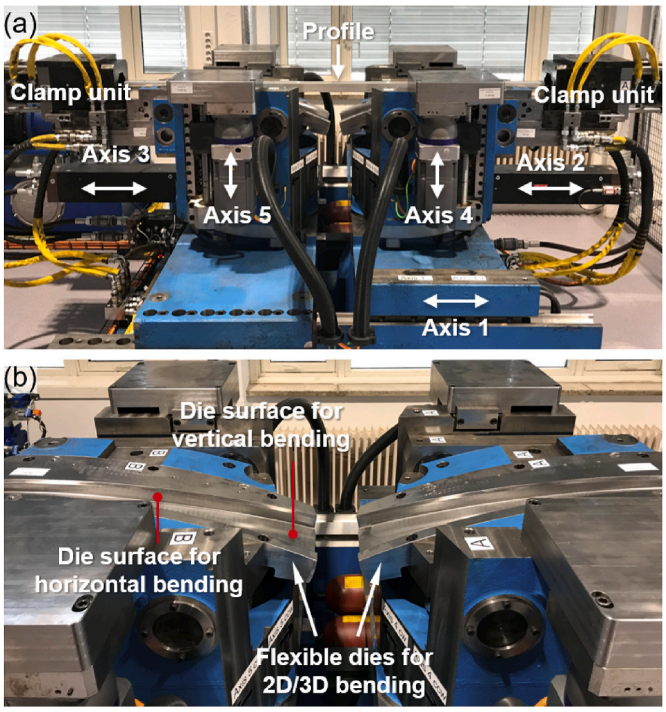

Fig. 5. Full scale, laboratory-based flexible stretch bending machine system: (a) overview of the machine; (b) flexible dies for 2D/3D bending.

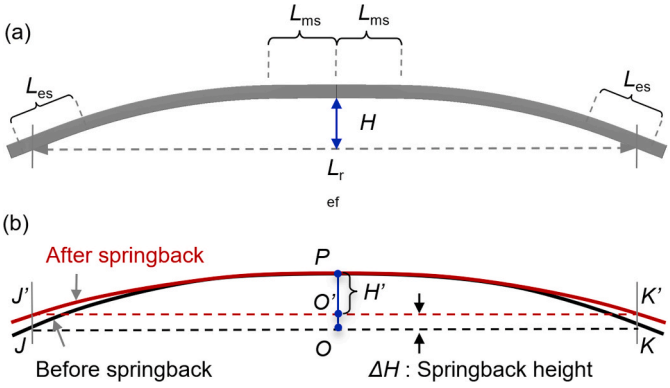

Fig. 6. Springback of stretch bending: (a) before unloading; (b) definition of springback.

symmetry point (P), taken from the inside of the profile. Similarly, the chord height (H') after springback is denoted as distance PO'. Thus, the springback chord height (ΔH) can simply be written by Eq. (1), which will be used in the following to evaluate the springback under different stretching conditions.

$$\Delta H = H - H' \tag{1}$$

3. Analytical model of stretch bending

3.1. Assumptions

Analytical modeling of the stretch bending process is developed under the following main assumptions:

- The cross-section of profile remains plane and perpendicular to the longitudinal axis after stretch bending.
- The stress state is uniaxial such that stresses across the thickness of members are neglected.
- Constant volume (mass conservation) principle is used for plastic deformation.
- The deformation theory of elasto-plasticity is employed.
- Large bending radius-to-depth of cross-section (Bernoulli-Navier) is assumed.

For the material properties used in the analysis, elasto-plasticity is used to describe the deformation behaviors upon forming. Since longitudinal strain component dominates deformation upon bending, it is taken to represent the total strain. The longitudinal strain can be written as follow:

$$\varepsilon = \varepsilon_e + \varepsilon_p \tag{2}$$

where ε_e is the elastic strain component, and ε_p is the plastic strain component expressed by $\varepsilon_p = \varepsilon - \varepsilon_e$. For purely elastic deformation, Hooke's law is used. When the material enters the plastic stage, a suitable constitutive relationship is selected in accordance with the deformation characteristics of the material used. Here the Swift hardening equation is employed to describe the true stress – (logarithmic) strain response. Thus, the constitutive model for elasto-plastic deformation can be written as:

$$\sigma_x = f(\varepsilon) = \begin{cases} E\varepsilon, & \varepsilon \le \varepsilon_e \\ K(\varepsilon_p + \varepsilon_0)^n, & \varepsilon > \varepsilon_e \end{cases} \tag{3}$$

where E is Young's modulus, K is the strength coefficient, n is the strain hardening exponent, and ε_0 is a coefficient of Swift hardening equation.

3.2. Geometry analysis

The formed profile includes geometry configurations of both bent and straight portions. Due to symmetry, a semi CAD model is used for analysis. As shown in Fig. 7, l_{ms}, l_b and l_{es} represent the lengths of the mid-depth layer of the mid-straight portion, bent portion, and end-straight portion, respectively.

In the stretch bending process considered, pre-stretching, in-process stretching, and post-stretching can be partially or completely applied. In this research, the total strain theory is assumed, meaning that the strain history does not influence the final strain distribution. Here the total stretch-induced tensile strain ($\bar{\varepsilon}^{gt}$) can be represented as:

$$\bar{\varepsilon}^{gt} = \varepsilon^{pre-t} + \varepsilon^{in-t} + \varepsilon^{post-t} \tag{4}$$

where ε^{pre-t}, ε^{in-t} and ε^{post-t} are the tensile strain components in the longitudinal direction caused by pre-stretch, in-process stretch and post-stretch, respectively. In order to represent the average global stretch level of the bent profile, the elongation of the centroid (mid-depth) layer is used for calculation, as shown in the following equation:

$$\bar{\varepsilon}^{gt} = \ln\left(1 + \frac{L_c - L_0}{L_0}\right) \tag{5}$$

where $\bar{\varepsilon}^{gt}$ is the average global stretching strain, L_0 is the initial length of profile, and L_c is the total length of the mid-depth layer after stretch bending, which can be calculated by:

$$L_c = l_{ms} + l_b + l_{es} \tag{6}$$

where l_b is the length of mid-depth layer of the bent portion, whichcan be calculated by:

$$l_b = \theta R_c \tag{7}$$

where θ is the bending angle, and R_c is the bending radius of the mid-depth layer.

As mentioned above, the tool configuration contains both bent and straight portions, so that the deformation of the profile in the longitudinal direction is nonuniform, especially within the transition zones

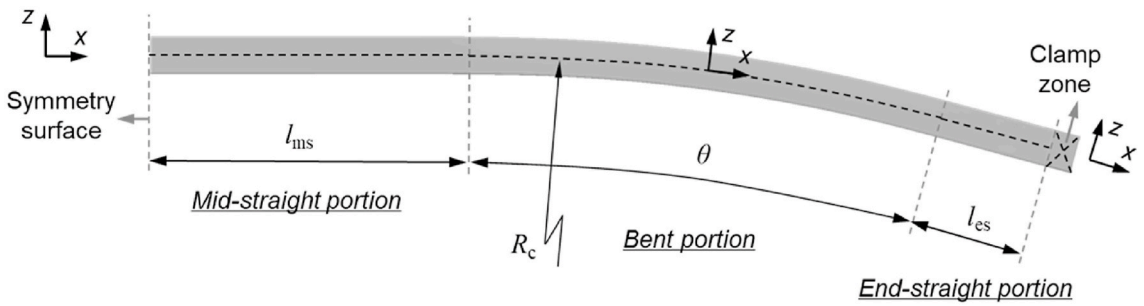

Fig. 7. Schematic view of formed profile with hybrid bent and straight configurations.

between the bent portion and the straight portions. In order to accurately characterize the strain distribution, the formed part is further divided into five different zones.

As shown in Fig. 8, the red and blue lines indicate the strain distributions of the outermost layer and innermost layer, respectively. The five zones are defined as follows:

- Mid-uniform stretch zone (MUS zone): This zone is in a uniform tensile state from *A* to *B*. The length of the MUS zone depends on the bent geometry as well as the stretch strain level. If the length of the mid-straight portion is very short, the MUS zone may not exist since the entire mid-straight portion appears within the transition state.
- Mid-transition zone (MT zone): This zone is in the transition state where the strain evolves from bending portion to mid-straight portion. It consists of a segment from *B* to *C* in the mid-straight portion, and an arc segment from *C* to *D* in the bent portion.
- Uniform bending zone (UB zone): This zone is in a uniform bending state, in which the bending deformations are constant from *D* to *E*.
- End-transition zone (ET zone): Like the MUS zone, the strain of this zone evolves from the bending portion to the end-straight portion. It also consists of a segment from *E* to *F* in the mid-straight portion, and an arc segment from *F* to *G* in the bent portion.
- End-uniform stretch zone (EUS zone): This zone resembles the MUS zone, and its length also depends on the final geometry of the bent part and applied stretch strain. If the straight end portion of the formed part is sufficiently short, the end-uniform stretch zone may not exist.

In order to identify the locations of the above-defined deformation zones, a local *x*-*z* coordinate system is defined and adopted throughout this paper. As shown in Fig. 8 (a), *x*-direction is defined in the longitudinal direction of bent profile, *y*-direction represents the width direction, and *z*-direction represents the depth direction. Point *A* in the symmetry plane is defined as the start point x=0. For the target geometry of the bent profile, the *x*-coordinates of points *C* and *F* are fixed. Consequently, the positions *B*, *D*, *E*, and G for the two transition zones must be identified. The length of the transition zone could be affected by the strain-stress gradient from the uniform bending zone to the mid-/end-uniform stretch zones. This gradient is governed by the depth of the profile, bending radius and the global stretch level.

Therefore, the coordinates of *B*, *D*, *E*, and *G* can be determined with respect to the total length of the mid-straight portion and end-straight portion. If the straight portion is sufficient long, a nominal length of the transition zone (l_{tr}) is first defined. As the transition is partially located in the mid portion and partially located in bending portion, a fraction parameter (η) is defined to divide the partial lengths of the transition zone located in two portions. The partial lengths located in straight and bent portions can thus be expressed as ηl_{tr} and $(1\text{-}\eta)l_{tr}$. Then,

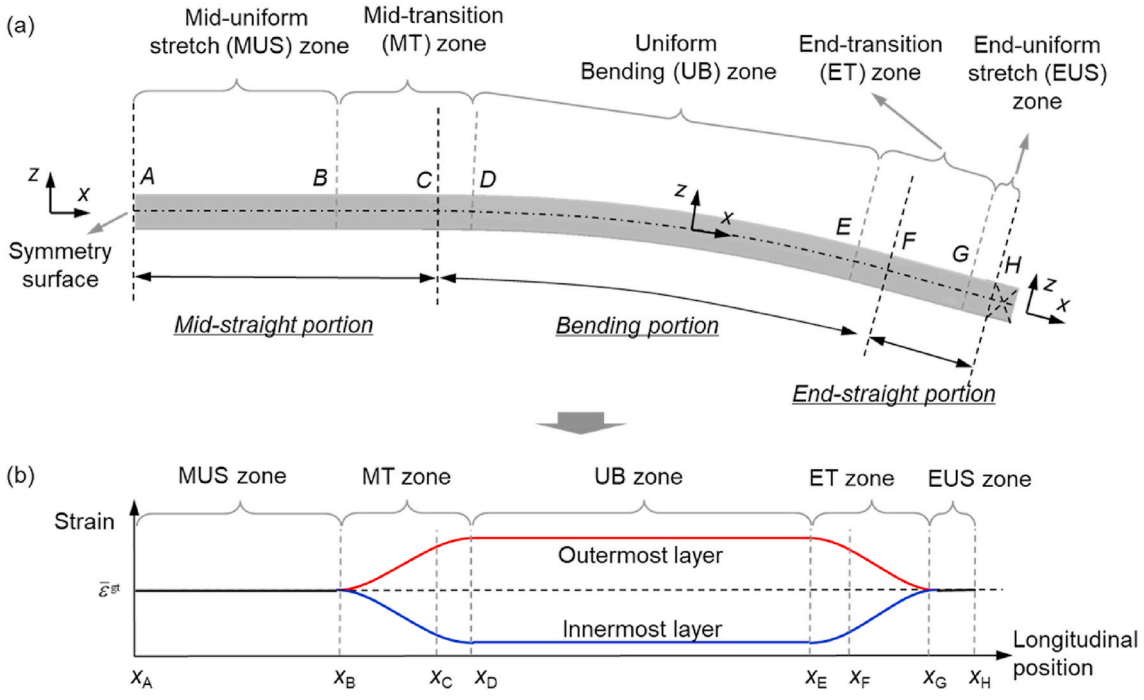

Fig. 8. Strain distribution of stretch bent profile: (a) deformation zones; (b) characteristics of strain distribution.

the coordinates of different deformation zones can be written as follows:

$$\begin{cases} x_A = 0 \\ x_B = l_{ms} - \eta l_{tr}, \ \text{if } l_{ms} \geq \eta l_{tr}; \ x_B = x_A, \ \text{else if } l_{ms} < \eta l_{tr} \\ x_C = l_{ms} \\ x_D = x_C + (1-\eta) l_{tr} \\ x_E = x_C + l_b - (1-\eta) l_{tr} \\ x_F = x_E + (1-\eta) l_{tr} \\ x_G = x_F + \eta l_{tr}, \ \text{if } l_{es} \geq \eta l_{tr}; \ x_G = x_F + l_{es}, \ \text{else if } l_{es} < \eta l_{tr} \\ x_H = x_G + (L_{es} - \eta l_{tr}), \ \text{if } l_{es} \geq \eta l_{tr}; \ x_H = x_G, \ \text{else if } l_{es} < \eta l_{tr} \end{cases} \tag{8}$$

where x_i $(i = A \sim H)$ represents the x-coordinate of the transition point between each deformation zone, l_{ms} and l_{es} are lengths of the mid-straight and end-straight portions, respectively.

3.3. Deformation analysis

3.3.1. Strain analysis for uniform stretching and uniform bending

As described in the previous section, the formed profile (see CAD model above) contains three different types of deformation zones; i.e., uniform stretching zones (MUS zone and EUS zone), uniform bending zone (UB zone) and bending-stretching transition zones (MT zone and ET zone), as shown Fig. 8. First, in the MUS zone and EUS zone, the stretch-induced longitudinal strain is considered equal to the average global stretch strain of the bent profile:

$$\varepsilon^t = \bar{\varepsilon}^{gt} = \ln\left(1 + \frac{L_c - L_0}{L}\right) \tag{9}$$

where ε^t denotes the longitudinal strain in uniform stretch zone, and $\bar{\varepsilon}^{gt}$ is the average global stretch strain given in Eq. (5).

Furthermore, the final longitudinal strain in zone UB is as a result of the combination of pure bending deformation and the applied stretching. Applying the principle of superposition, as shown in Fig. 9, the longitudinal strain of the UB zone can be expressed as the sum of the strain component induced by pure bending and the strain component induced by stretching:

$$\varepsilon^b = \varepsilon^{pb} + \bar{\varepsilon}^{gt} \tag{10}$$

where ε^b is the longitudinal strain in the UB zone, ε^{pb} is the longitudinal strain component induced by pure bending, and ε^t is the longitudinal strain component induced by stretching mentioned in Eq. (9).

As shown in Fig. 9 (a), the longitudinal strain component $\varepsilon^{pb}(z)$ induced by pure bending at an arbitrary position (z) across the depth of the cross-section can be calculated as:

$$\varepsilon^{pb}(z) = \ln(1 + d_z/\rho) = \ln\left(1 + \frac{z - z_{nl}}{R_c + z_{nl}}\right) \tag{11}$$

where ρ is the bending radius of the neutral layer, and d_z is the distance taken perpendicular from the identified position of the NL to any point (z) in the plane of the cross-section, and R_c is the bending radius taken from the curvature center to the mid depth of the profile. In this equation, the centroid of the profile is used as the zero-reference point, and the z-coordinate of the NL location is denoted z_{nl}. In this study, the bending radius is much larger than the profile depth ($R_c/h = 45.68$) so that the NL shifting can be ignored. Thus, in the analytical model, the longitudinal strain component induced by pure bending can be re-written as:

$$\varepsilon^{pb}(z) = \ln(1 + z/R_c) \tag{12}$$

By substituting Eqs. (9) and (12) into Eq. (10), the final longitudinal strain $\varepsilon^b(z)$ in the UB zone can be calculated as:

$$\varepsilon^b(z) = \varepsilon^t + \varepsilon^{pb}(z) = \ln\left(1 + \frac{z}{R_c}\right) + \ln\left(1 + \frac{L_c - L_0}{L_0}\right) \tag{13}$$

3.3.2. Strain analysis for bending-stretching transition

3.3.2.1. Governing equation for bending-stretching transition length. As the strain distributions in MUS, EUS and UB zones have been determined in Section 3.3.1, the strain gradient and stress gradient between UB zone and MUS (or EUS) zone are known. As shown in Fig. 8, the strain distribution of the outermost layer is used as an example to analyze the stretching-dependent stress gradient between UB zone and MUS (or EUS) zone. Due to the flattening of the stress-strain curve towards higher strains, the stress difference within a given strain interval is reduced, as shown in Fig. 10. Therefore, the stress gradient between UB and MUS (or

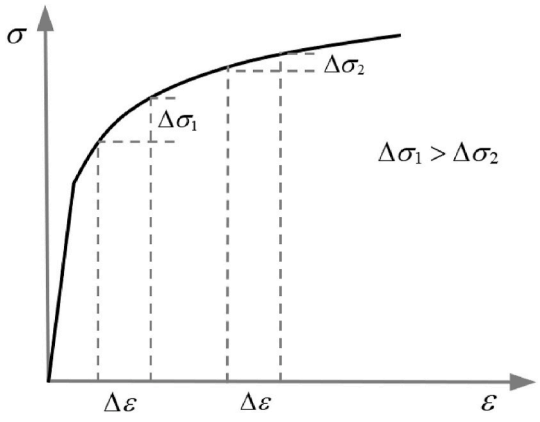

Fig. 10. Stress gradient across the depth of profile under different stretching levels.

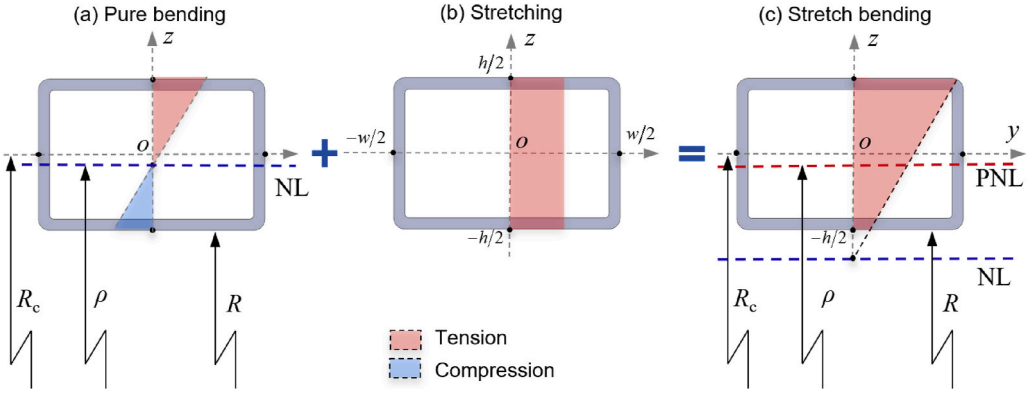

Fig. 9. Strain superposition principle: (a) pure bending induced nonuniform tension-compression strain; (b) stretching-induced uniform tension strain; (c) strain superposition of pure bending and stretching.

EUS) zone will be reduced at higher stretching strain level, even though the strain gradient across the depth of bent profile remains unchanged. In addition, the lower the stress difference, the shorter the length of the transition zone from the bent portion to the straight portions. Consequently, the length of the bending-stretching transition zone can be assumed proportional with the stress difference between UB zone and MUS (or EUS) zone. As this stress difference approximately equals to half the stress difference between the outermost and innermost layer across the profile depth, the length of the bending-stretching transition zone can be expressed as:

$$l_{tr} \propto \Delta\sigma \tag{14}$$

where the length of bending-stretching transition zone (l_{tr}), and $\Delta\sigma$ is the stress difference between the outermost and innermost layers of the cross-section.

As the strain gradient across the depth remains unchanged, the stress difference across the depth is only affected by the average global stretch level given by Eq. (5). As shown in Fig. 10, when the average global stretch strain increases, the stress gradient decreases. Accordingly, the length of the bending-stretching transition can be assumed to be proportional with the stress (equals the stress of MUS and EUS zones), corresponding to the average global stretch level.

Here a Ludwik-type function is employed to rewrite the stress-strain curve:

$$\frac{\overline{\sigma}^{gt}}{\sigma_0} = 1 + \frac{K_\sigma}{\sigma_0}\left(\overline{\varepsilon}_p^{gt}\right)^{n_\sigma} \tag{15}$$

where $\overline{\sigma}^{gt}$ represents the average tensile stress, K_σ and n_σ are the strength coefficient and straining hardening exponent fitted to the Ludwik model, respectively, σ_0 is the previously defined as initial yield stress, and $\overline{\varepsilon}_p^{gt}$ is the plastic strain caused by average global stretching, which can be calculated by $\overline{\varepsilon}_p^{gt} = \overline{\varepsilon}^{gt} - \sigma^0/E$.

Based on above analysis, a similar function is constructed to describe the stretching-dependent length of the transition zone:

$$\frac{l_{tr}}{l_{tr,0}} = 1 - \frac{K_l}{l_{tr,0}}\left(\overline{\varepsilon}_p^{gt}\right)^{n_l} \tag{16}$$

where $l_{tr,0}$ is a constant parameter, and K_l is a parameter controlling the change of length with respect to the stretching strain, and n_l is an exponent controlling the change rate of the transition length. It is noted that the constant parameter $l_{tr,0}$ is assumed to be an independent parameter, which denotes the length of the bending-stretching transition zone when the applied global stretching strain upon bending vanish (i.e., no stretching applied during bending). In other words, $l_{tr,0}$ is a maximum-length condition as the stress difference is at maximum when no stretching is applied during bending. Based on above analysis, the length of the transition zone can be assumed proportional to the stress of MUS or EUS zones, such that the following relationships can be assumed: $K_\sigma/\sigma_0 = K_l/l_{tr,0}$, and $n_l = n_\sigma$. Accordingly, the governing equation for the transition length is constructed as follow:

$$l_{tr} = l_{tr,0}\left(2 - \overline{\sigma}^{gt} / \sigma^0\right) \tag{17}$$

In this work, the length of the bending-stretching transition is assumed to be equal to ten times the profile depth, namely, $l_{tr,0} = 10h$. As for the fraction parameter (η) in Eq. (8), the partial lengths of the transition zones located in bent and straight portions are analytically estimated to be 2:1 for the forming case in Section 5 based on an assumed Coulomb friction coefficient of 0.33, reflecting low degree of lubrication. Alternatively, for more precise evaluation, $l_{tr,0}$ can either be determined by using simulation or inversely calibrated by experiment.

3.3.2.2. Governing equation for strain distribution. At the beginning of the analysis, it should be noted that superscript 'x', which represents the strain component in the longitudinal direction (x-direction), is introduced in the following equations to distinguish the strain components in y-direction and z-direction (as shown in Figs. 8 and 9) for the representation of material anisotropy in the deformation analysis. In order to describe the strain evolution of the outermost layer in the transition regions, a simple linear equation is constructed. Thus, the strain of MT zone can be written as:

$$\varepsilon_{BD}^{x,o}(x) = \varepsilon_D^{x,o} - \frac{\varepsilon_D^{x,o} - \varepsilon_B^{x,o}}{l_{tr}}\left(-x + x_D\right) \tag{18}$$

where the superscript 'o' denotes the outermost layer, $\varepsilon_{BD}^{x,o}(x)$ is the longitudinal strain of the outermost layer in the transition zone, $\varepsilon_B^{x,o}$ and $\varepsilon_D^{x,o}$ are the longitudinal strains of outermost layer at points B and D, respectively.

Similarly, the strain evolution of the innermost layer can be given by:

$$\varepsilon_{BD}^{x,i}(x) = \varepsilon_D^{x,i} - \frac{\varepsilon_D^{x,i} - \varepsilon_B^{x,i}}{l_{tr}}\left(-x + x_D\right) \tag{19}$$

where the superscript 'i' represents the innermost layer. As section B is located at the end of the MUS zone, both the outermost and innermost strains are equal to the average global stretch strain (ε^t). Section D is located at the start of the UB zone, which means that the outermost and innermost strains can be calculated as follows:

$$\begin{cases} \varepsilon_D^{x,o} = \ln\left(1 + \dfrac{h}{2R_c}\right) + \ln\left(\dfrac{L_c}{L_0}\right) \\ \varepsilon_D^{x,i} = \ln\left(1 - \dfrac{h}{2R_c}\right) + \ln\left(\dfrac{L_c}{L_0}\right) \end{cases} \tag{20}$$

Since the strain distribution across the depth of the section can be assumed linear (Bernoulli-Navier), the strain at an arbitrary depth of profile can be calculated:

$$\varepsilon_{BD}^{x}(x,z) = \varepsilon_{BD}^{x,i}(x) + \frac{\varepsilon_{BD}^{x,o}(x) - \varepsilon_{BD}^{x,i}(x)}{h}\left(z - \frac{h}{2}\right) \tag{21}$$

where $\varepsilon_{BD}^{x}(x,z)$ represents the strain at coordinate z in section-x.

Similarly, for zone ET between E and G, the strain at an arbitrary z-position in section-x can be calculated as follow:

$$\varepsilon_{EG}^{x}(x,z) = \varepsilon_{EG}^{x,i}(x) + \frac{\varepsilon_{EG}^{x,o}(x) - \varepsilon_{EG}^{x,i}(x)}{h}\left(z - \frac{h}{2}\right) \tag{22}$$

where $\varepsilon_{EG}^{x,o}(x)$ and $\varepsilon_{EG}^{x,i}(x)$ represent the strain at the outermost and innermost layers in zone ET, expressed by:

$$\begin{cases} \varepsilon_{EG}^{x,o}(x) = \varepsilon_E^{x,o} - \dfrac{\varepsilon_E^{x,o} - \varepsilon_G^{x,o}}{l_{tr}}\left(x - x_E\right) \\ \varepsilon_{EG}^{x,i}(x) = \varepsilon_E^{x,i} - \dfrac{\varepsilon_E^{x,i} - \varepsilon_G^{x,i}}{l_{tr}}\left(x - x_E\right) \end{cases} \tag{23}$$

Here section G is located at the start of zone EUS, and both the outermost and innermost strains are equal to the average global stretch strain ($\overline{\varepsilon}^{gt}$). Reference point E is located at the end of the UB zone, which means that the outermost and innermost strains can also be calculated by Eq. (20).

Finally, the governing equation for the longitudinal strain distribution within the entire bent profile can be represented by Eq. (24) in a local x-z coordinate system:

$$\varepsilon^{x}(x,z)=\begin{cases}\varepsilon^{t}, \text{ MUS zone}: \ 0\le x<x_B\\ \varepsilon_{BD}^{x,i}(x)+\dfrac{\varepsilon_{BD}^{x,o}(x)-\varepsilon_{BD}^{x,i}(x)}{h}\left(z-\dfrac{h}{2}\right), \text{ MT zone}: \ x_B\le x<x_D\\ \ln\left(\dfrac{z}{R_c}\right)+\ln\left(\dfrac{L_c-L_0}{L_0}\right), \text{ UB zone}: \ x_D\le x<x_E\\ \varepsilon_{EG}^{x,i}(x)+\dfrac{\varepsilon_{EG}^{x,o}(x)-\varepsilon_{EG}^{x,i}(x)}{h}\left(z-\dfrac{h}{2}\right), \text{ ET zone}: \ x_E\le x<x_F\\ \varepsilon^{t}, \text{ EUS zone}: \ x_G\le x\le x_H\end{cases} \tag{24}$$

Considering the anisotropy of the extruded profile, the Lankford coefficient (r-value) along the extrusion direction is used to analyze the plastic strain in the local y-direction (width direction) and local z-direction (depth direction). Here the same r-value is assumed for both inner/outer flanges and left/right webs. The elastic deformation is ignored in analyzing the changes of thickness, width and depth of the formed profile. Thus, when demanding volume conservation, the strain component $\varepsilon^{y}(x,z)$ in the y-direction can be written as follows:

$$\varepsilon^{y}(x,z)=\begin{cases}-\dfrac{r}{1+r}\varepsilon^{x}(x,z), \text{ flanges}\\ -\dfrac{1}{1+r}\varepsilon^{x}(x,z), \text{ sidewalls}\end{cases} \tag{25}$$

where r is the r-value obtained in tensile experiments of samples cut in the extrusion direction.

Similarly, the strain component $\varepsilon^{z}(x,z)$ in the z-direction can be calculated by:

$$\varepsilon^{z}(x,z)=\begin{cases}-\dfrac{1}{1+r}\varepsilon^{x}(x,z), \text{ flanges}\\ -\dfrac{r}{1+r}\varepsilon^{x}(x,z), \text{ sidewalls}\end{cases} \tag{26}$$

By combining Eqs. (24)–(26) and Eq. (3), the stress distribution $\sigma(x,z)$ of the entire formed profile can thus be solved analytically.

4. Analytical model of springback

4.1. Full moment (FM) – curvature relation

To analytically calculate springback after unloading, a moment-curvature model needs to be developed for the stretch bending process. Recalling the theory of elasto-plastic bending [40], the following equation can be obtained applicable for the unloading process:

$$\Delta\kappa=\kappa_0-\kappa_u=\frac{\Delta M}{EI}=\frac{M_{ep}}{E\cdot I} \tag{27}$$

where $\Delta\kappa$ is the change of bending curvature upon unloading, κ_0 and κ_u are curvatures before and after unloading, respectively, M_{ep} is the applied moment prior to unloading, E is Young's modulus, and I is the second moment of area of the cross-section.

As previously discussed, the curvatures vary along the part and are generally different from the tool curvature in the transition regions. Thus, in addition to the internal moment in the main bending portion, the internal moment distribution in other portions will also contribute to the final springback, as illustrated by the shaded moment area in Fig. 11. Therefore, a full moment - curvature model must be constructed to include the springback contribution of the internal moment from all sections along the profile.

For this purpose, the moment function along the entire profile including the previously-defined various deformation zones, i.e., UB zone, MUS zone, EUS zone, MT zone and ET zone, must be constructed. This is given by:

$$M(x)=\int_{z=z_i}^{z=z_o}\sigma(x,z)\cdot z\,dA \tag{28}$$

where $M(x)$ represents the moment function in the longitudinal direction of formed profile, and dA is the integration area. Based on the strain analysis in Section 3.3, the integration area can be written as follows:

$$dA=\begin{cases}w_0\exp[\varepsilon^{y}(x,z)]dz, \ z_i\le z\le z_{is}, \text{ inner flange}\\ 2t_0\exp[\varepsilon^{y}(x,z)]dz, \ z_{is}<z<z_{os}, \text{ sidewalls}\\ w_0\exp[\varepsilon^{y}(x,z)]dz, \ z_{os}\le z\le z_o, \text{ outer flange}\end{cases} \tag{29}$$

where w_0 and t_0 are the initial width of inner/outer flanges and thickness of sidewall, respectively, z_i, z_o, z_{is}, z_{os} are the four reference coordinates of the section after forming, as shown in Fig. 12, which represent the innermost and outermost positions of the cross section, and the innermost and outermost positions of sidewalls. The four reference coordinates can be expressed as follows:

$$\begin{cases}z_i=-h_{side,in}-t_{in}\\ z_{is}=-h_{side,in}\\ z_{os}=h_{side,out}\\ z_o=h_{side,out}+t_{out}\end{cases} \tag{30}$$

where t_{in} and t_{out} are the thickness of the inner and outer flanges, respectively, $h_{side,in}$ and $h_{side,out}$ are the heights of the inner and outer half sidewalls, respectively, and can be calculated as follows:

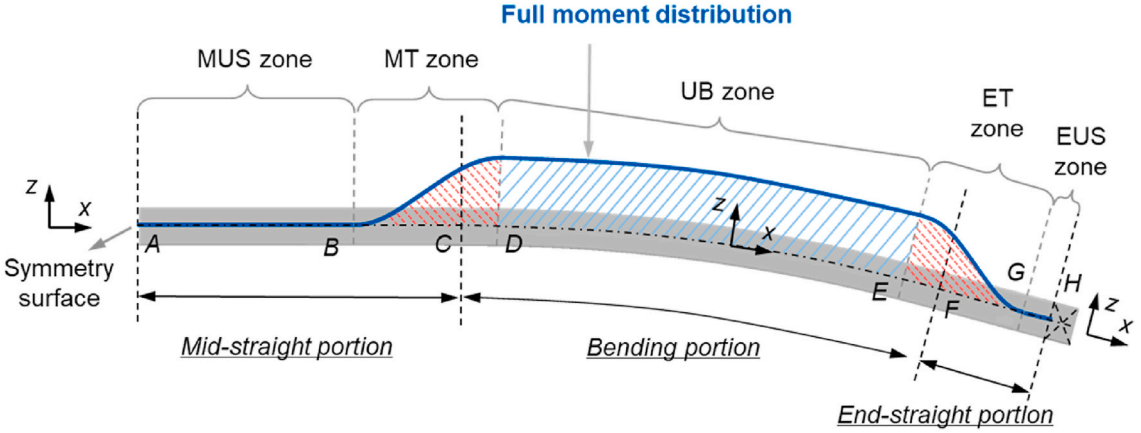

Fig. 11. Full moment distribution of the entire formed profile.

$$\begin{cases} t_{\text{in}} = \int_{-h/2}^{-h/2+t} t\exp[\varepsilon^z(x,z)]dz, \text{ inner flange} \\ h_{\text{side,in}} = \int_{-h/2+t}^{0} w\exp[\varepsilon^z(x,z)]dz, \text{ inner half sidewalls} \\ h_{\text{side,out}} = \int_{0}^{h/2-t} w\exp[\varepsilon^z(x,z)]dz, \text{ outer half sidewalls} \\ t_{\text{out}} = \int_{h/2-t}^{h/2} t\exp[\varepsilon^z(x,z)]dz, \text{ outer flange} \end{cases} \tag{31}$$

Then, the curvature – moment relation shown in Eq. (27) can be re-written as follow:

$$\Delta\kappa(x) = \frac{M(x)}{E \cdot I(x)} \tag{32}$$

where $\Delta\kappa(x)$ is the curvature during unloading, $I(x)$ is the second moment of inertia at section-x of the deformed profile after stretch bending. Due to the forming-induced changes of thickness, width and depth of profile, the second moment of area can be calculated by:

$$I(x) = w_{\text{avg}} h_{\text{avg}}{}^3 / 12 - \left(w_{\text{avg}} - 2t_{\text{side,avg}}\right)\left(h_{\text{avg}} - 2t_{\text{flange,avg}}\right)^3 / 12 \tag{33}$$

where w_{avg}, $t_{\text{flange,avg}}$, $t_{\text{side,avg}}$ and h_{avg} represent the average width, thickness of inner/outer flange, thickness of left/right sidewalls, and depth after bending, respectively. Using the average global stretch strain, the average width, thicknesses and depth can be calculated as follows:

$$\begin{cases} w_{\text{avg}} = w\exp\left(-\dfrac{r}{1+r}\bar{\varepsilon}^{\text{gt}}\right) \\ t_{\text{flange,avg}} = t\exp\left(-\dfrac{1}{1+r}\bar{\varepsilon}^{\text{gt}}\right) \\ t_{\text{side,avg}} = t\exp\left(-\dfrac{1}{1+r}\bar{\varepsilon}^{\text{gt}}\right) \\ h_{\text{avg}} = 2t_{\text{flange,avg}} + (w-2t)\exp\left(-\dfrac{r}{1+r}\bar{\varepsilon}^{\text{gt}}\right) \end{cases} \tag{34}$$

Hence, as shown in Fig. 13, the springback angle, considering the nonuniformly distributed full moment along the entire formed profile, can be analytically calculated:

$$\Delta\theta = \int_{x=x_A}^{x=x_H} \Delta\kappa(x)dx = \sum \Delta\alpha_i = \int_{x_A}^{x_B} 0dx + \underbrace{\int_{x_B}^{x_C} \Delta\kappa(x)dx + \int_{x_C}^{x_D} \Delta\kappa(x)dx}_{\text{Contribution by bending-stretching (mid) transition zone}} + \underbrace{\int_{x_D}^{x_E} \Delta\kappa(x)dx}_{\text{Contribution by uniform bent zone}} + \underbrace{\int_{x_E}^{x_F} \Delta\kappa(x)dx + \int_{x_F}^{x_G} \Delta\kappa(x)dx}_{\text{Contribution by bending-stretching (end) transition zone}} + \int_{x_G}^{x_H} 0dx \tag{35}$$

where $\Delta\alpha_i$ denotes the contributions of different deformation zones to the final global springback angle as defined by the change of slope of the part's end upon unloading.

As described in Section 2.2, the curvature of the formed profile after unloading is varying between bent, transition and straight zones. This means that springback offset (chord height) cannot be described by using the springback change of slope (overall bend angle). Therefore, a relationship between the chord springback chord height and the full moment distribution must be established. For this purpose, the virtual work method is employed. As shown in Fig. 13 (a), the nonuniform distribution of moment induces nonuniform change of curvatures from

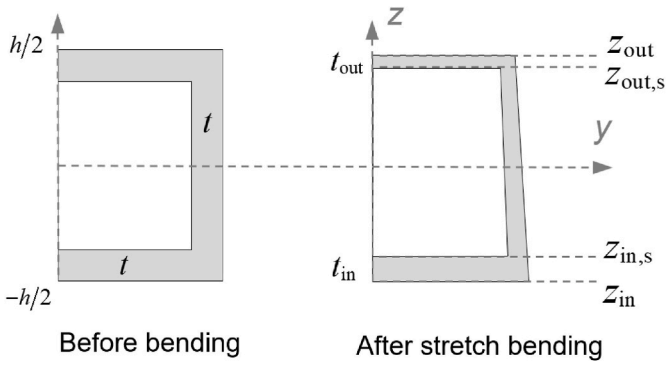

Fig. 12. Variations of thickness, width and depth of profile during stretch bending due to mass conservation upon plastic deformation.

A to H during unloading. Using the virtual work method, the total springback chord height (δ) from A to H can be calculated as follow:

$$\delta = \int_{x_A}^{x_H} \Delta\kappa(x) \cdot M^{\text{v}}(x)dx \tag{36}$$

where $M^{\text{v}}(x)$ is the virtual moment function obtained by applying a virtual unit load in the vertical direction at point H, while the semi-profile is fully clamped in the center A, as shown in Fig. 13 (b).

According to the geometry relation illustrated in Fig. 13 (b), the virtual moment distribution function from A to H can be expressed by:

$$M^{\text{v}}(x) = \begin{cases} x - x_A, \ x_A \le x < x_B, \text{ MUS zone} \\ \left.\begin{array}{l} x - x_A, \ x_B \le x < x_C \\ (x_C - x_A) + R_c\sin((x-x_C)/R_c), \ x_C \le x < x_D \end{array}\right\}, \text{ MT zone} \\ (x_C - x_A) + R_c\sin((x-x_C)/R_c), \ x_D \le x < x_E, \text{ UB zone} \\ \left.\begin{array}{l} (x_C - x_A) + R_c\sin((x-x_C)/R_c), \ x_E \le x < x_F \\ (x_C - x_A) + R_c\sin\theta + (x-x_F)\cos\theta, \ x_F \le x < x_G \end{array}\right\}, \text{ ET zone} \\ (x_C - x_A) + R_c\sin\theta + (x-x_F)\cos\theta, \ x_F \le x \le x_H, \text{ EUS zone} \end{cases} \tag{37}$$

4.2. Solving procedure

The full moment (FM) model established above includes a set of complex integrals. It is impossible to obtain an explicit analytical solution, so a numerically-assisted procedure is needed. As shown in Fig. 14, for a given section geometry **S** and bending configuration **B**, solving for springback offset includes four steps as follows:

- Step 1: Determine the average global stretching level and the strain distributions in the bending zones and stretching zones.
- Step 2: Identify the lengths of bending-stretching transition zones and the reference coordinates of different deformation zones, and thus calculate distributions of strain and stress along the entire profile
- Step 3: Determine the instantaneous thickness, width and depth of the formed profile, and then calculate full moment – curvature relationship.

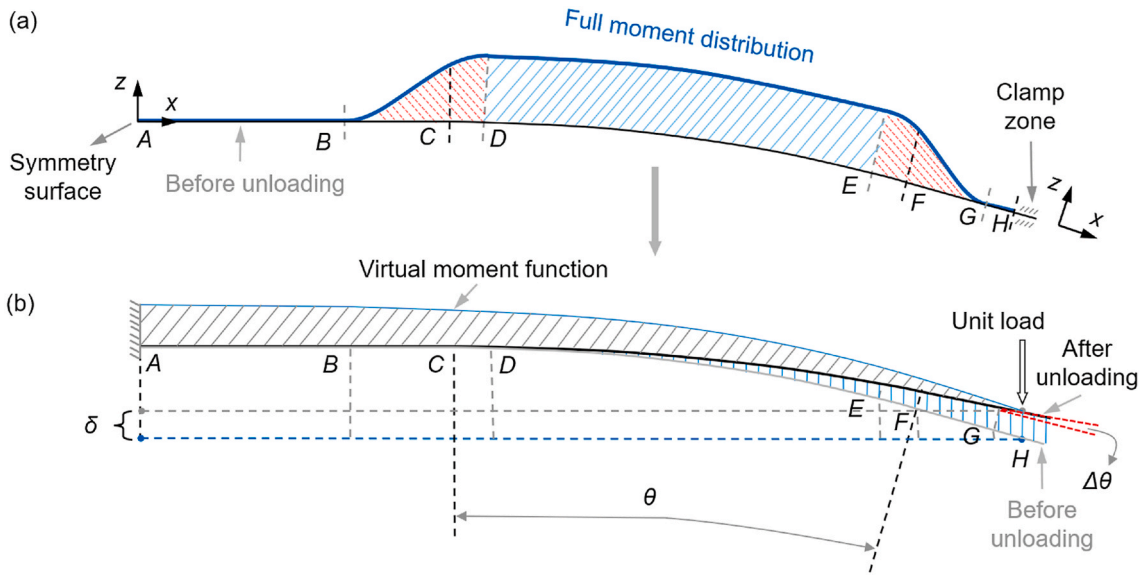

Fig. 13. Analysis of springback chord height: (a) formed profile before unloading; (b) virtual work method for springback chord height calculation.

- Step 4: Determine the springback chord height through the virtual work method, as described above.

A numerical integration approach using a forward Euler algorithm was employed to solve the analytical model, which was coded and implemented based on MATLAB R2019b.

5. Validation and discussion

5.1. Experiments and numerical modeling

AA6082-T4 rectangular, hollow extrusions are used in the experiments. The width is 60 mm, the depth is 40 mm, the gauge thickness is 3 mm, and the outer and inner fillet radii are 2 mm and 1 mm, respectively. By conducting tensile tests of samples cut from the middle zone of the top of the profile, the stress-strain curve is obtained, as shown in Fig. 15. The gauge length and width of the tensile sample are 50 mm and 10 mm, respectively. Three repeated tests are carried out and the Digital Image Correlation method is used to measure the full field strain distribution of the gauge area. The r-value is determined at a reference longitudinal strain of 2.0%. The basic mechanical properties are obtained as follows: elastic modulus is $E = 71{,}982$ MPa, the 0.2% offset proof stress (initial yield stress) is $\sigma_0 = 146$ MPa, the ultimate tensile strength is $\sigma_b = 266$ MPa, and the r-value is 0.41, indicating high normal anisotropy. The Swift hardening function is employed to describe the stress-strain relationship. It can be found from Fig. 15, showing that the fitted curve can well describe the stress-strain relationship. The hardening exponent (n) and strength coefficient (K) fitted to the Swift equation are $n = 0.26$, and $K = 502$ MPa, respectively.

A series of carefully designed experiments, applying different stretch strain levels, is conducted to validate the forming process and the developed analytical springback model. In the stretch bending process, the profile is initially stretched to a pre-set length (1900 mm), and then followed by a combined stretch-bending operation. It should be noted that the geometric locations of the pivots will induce a stretch strain of 2.05% during the combined stretch-bending operation, without the initial pre-stretching applied; that is, the total stretch strain is composed of the additional strain induced by pre-stretching and the strain induced by the rotational movement creating combined stretch-bending.

As shown in Table 1, five sets of total stretching levels are used in the experiments. The as-received profiles are cut into different pre-set lengths to realize the pre-set stretching levels with the exact same configuration prior to unloading. For comparing the impact of applied stretching level on springback, the configuration of the bent parts prior to unloading was exactly the same, independent of the (pre-) stretching sequence. As shown in Fig. 7, the length of the mid-straight portion is $l_{ms} = 44.20$ mm, the length of end-straight portion is $l_{es} = 106.30$ mm, the bending radius of center line is $R_c = 1827$ mm, and the bending angle is $\theta = 24.6^\circ$. In order to examine the process capability of this stretching-controlled forming method, 10 repeated tests are performed for the stretch strain levels of 2.05% and 4.15%. For the other sets, three repeated tests are conducted. Mobil Vactra™ lubrication oil No. 2 is used to lubricate the contact surfaces between the profile and the tools. The control loading time for pre-stretching and bending are calculated and shown in Table 1.

Fig. 16 (a) shows the experimentally formed parts for all five sets of different stretching levels. The bent profile is measured using a special-purpose laboratory fixture. As shown in Fig. 16 (b) ~ (d), the fixture is composed of two pre-calibrated reference points with the reference distance of $L_{ref} = 1764$ mm, and a pre-calibrated digital measuring scale. By adding the recorded value to the calibration height, the chord height after springback can thus be obtained. For the target geometrical dimension in the experiments—provided by the stop configuration of the tools—as shown in Fig. 7, the chord height before unloading (H) is calculated as 203.17 mm. Consequently, the springback height can be obtained from Eq. (1).

In addition, several preliminary FE simulations have been carried out to evaluate mechanisms important to the assumptions made in the FM analytical model, as well as explore the more general deformation characteristics of the forming process. Based on the Abaqus R2017x, a full-process FE model of stretching-bending-unloading is established. Here the forming (stretching-bending) and unloading steps are modeled by the explicit and implicit solvers, respectively. As shown in Fig. 17, the half model is used due to symmetry. The forming dies, clamp tools and inserts are modeled as discrete, rigid bodies and meshed by element type R3D4, while the profile is meshed by element type C3D8R with a size of $4 \times 3 \times 1$ mm. The Coulomb friction law with coefficient of 0.2 is used to model friction between the profile and tools. Hooke's law and J2 plasticity model, which are calibrated by the tensile test, are used to model the elasto-plastic response of the profile. Like the analytical models, a local coordinate system is employed to define the material orientation in the simulation. The unloading process was initiated by releasing contact and removing tools from the formed part while fixed constraints are applied at the symmetry plane.

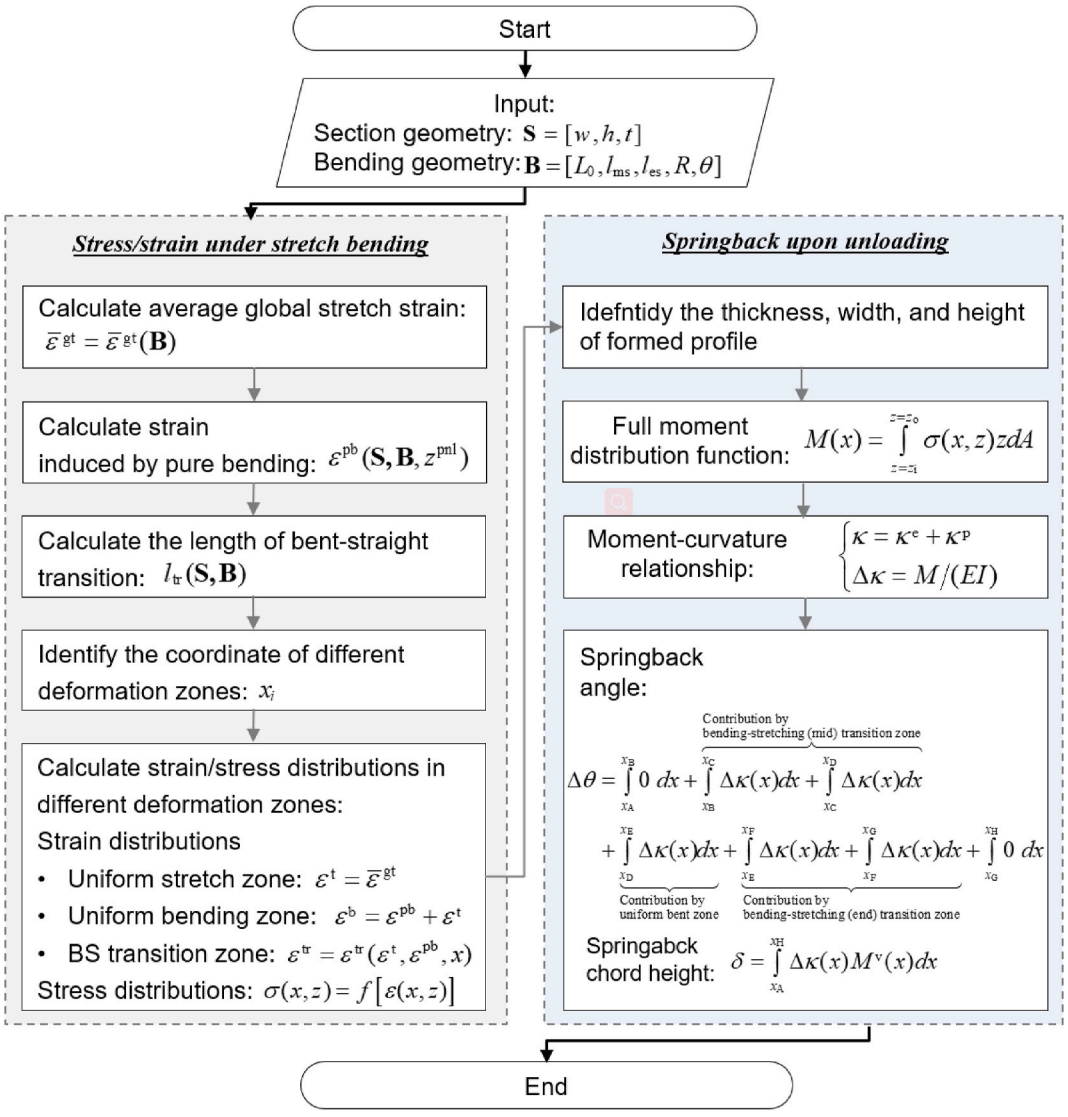

Fig. 14. Solving procedure of the FM springback model.

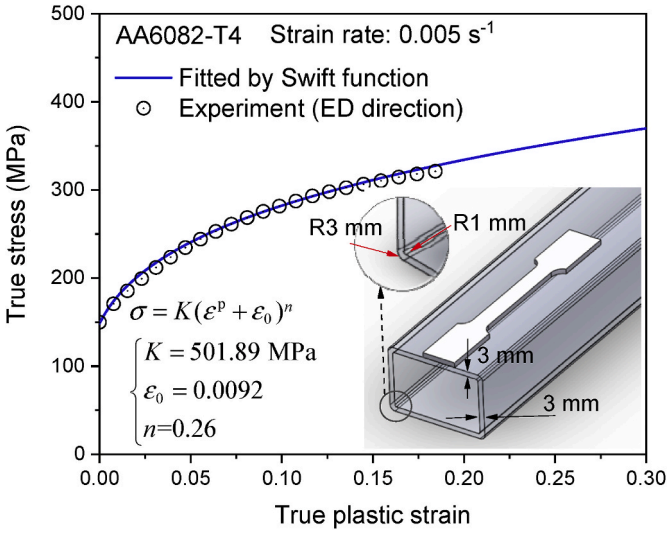

Fig. 15. True stress – true strain curves of AA6082-T4 profile.

5.2. Validation of stretching-controlled forming processes

Based on the experimental procedure described above, the dimensional capability of the forming sequenced with different stretch levels is validated. As shown in Fig. 18 (a), taking the bending processes with stretch strain levels of 2.05% and 4.15% as examples, the repeatability of the newly-developed process and machine is validated. The average absolute errors of chord heights under stretching strains of 2.05% and 4.15% are 0.20 mm and 0.15 mm, respectively, and the standard deviations for the above two stretching levels are 0.26 and 0.17, respectively. It is found that the forming process and established machine system can provide high dimensional part accuracy. Here, for the purpose of industrial comparison, the process capability can be predicted for a more quantitative analysis, as shown in the following equation:

$$C_p=\frac{\mathrm{USL}-\mathrm{LSL}}{6\cdot\mathrm{SD}} \tag{38}$$

where C_p represent the process capability, 'USL' and 'LSL' represents the upper and lower specification limits, respectively, and 'SD' is the standard deviation of chord heights of the ten samples for each set.

Assuming that tolerance band is ULS – LSL = 2 mm (±1 mm)—which in industrial terms is a very tight tolerance for such a large-size part—the process capabilities for bending with stretching strains of 2.05% and

Table 1
Parameters used in forming experiments.

No.	Totally applied stretch strain	Nominal input initial length of profile [mm]	Average length of cut samples [mm]	Additional stretching displacement [mm]	Pre-stretching loading time [s]	Bending loading time [s]	Repeated times
1	2.05%	1900.00	1900.00	0	0	15.07	10
2	2.55%	1891.10	1891.00	8.90	5.48	15.07	3
3	3.01%	1883.10	1882.93	16.90	10.33	15.07	3
4	3.58%	1873.43	1873.43	26.57	16.32	15.07	3
5	4.15%	1863.47	1863.21	36.53	22.57	15.07	10

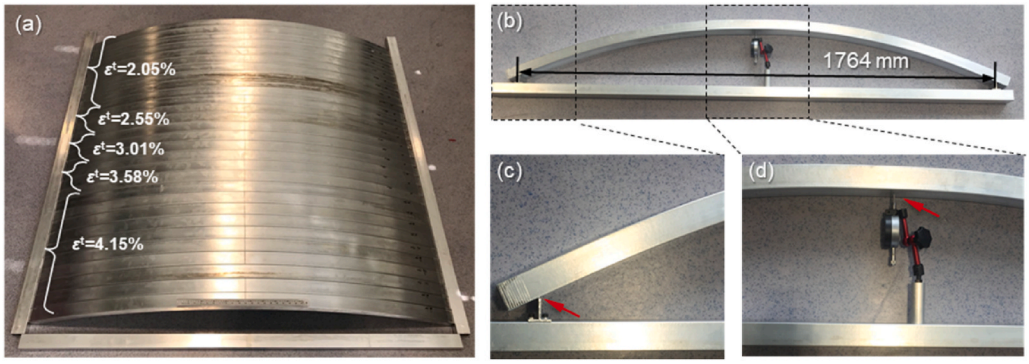

Fig. 16. Experimental samples and springback measurement fixture: (a) bent profiles; (b) overview of springback measurement; (c) reference point; (d) measurement point.

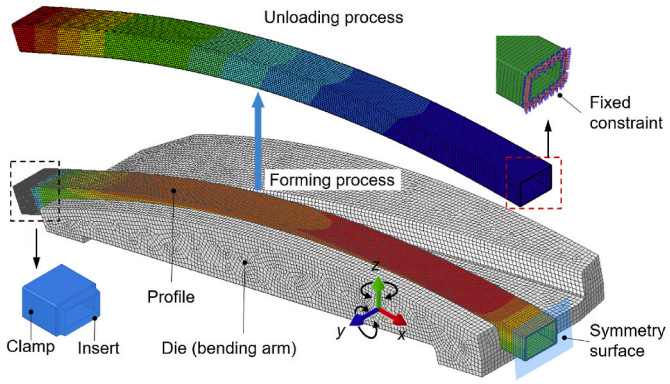

Fig. 17. FE modeling of stretch bending process.

4.15% are 1.26 and 1.98, respectively. A reference value of $C_p = 1.33$ is considered to represent acceptable process capability for standard characteristics in e.g., the automotive industry, as well as to be a 'ideal' target in terms of OEE [41]. From this point of view, the process capability under the lower stretching level with 2.05% is next to industrial standards. Moreover, although the sample size is small it is interesting to note that the higher stretching level of 4.15% provides a significant improvement, making the process capability higher than this reference. Thus, it can be found that this new, flexible forming process can achieve high dimensional capability. In addition, the process capability can be improved when forming at higher stretching level up to a certain range, which is of importance for defining the optimal forming sequences with regard to dimensional forming accuracy.

Comparing the springback under different stretching levels, as shown in Fig. 18 (b), the springback chord height is reduced by about 32% from 6.37 mm to 4.32 mm, when the stretch strain increases from 2.05% to 4.15%. It can also be found that the increasing rate trends to be lower with increased stretching strains. Even though all the experiments are in Mode 5 (as shown in Fig. 2), the observed reduction of springback is still considerable throughout the entire stretching strain range investigated. For the stretch-strain controlled bending process, with the continuous increase of stretch strain, the stress gradient across the depth of profile is reduced and the rate of springback trends to decrease. However, the increased stretch strain can simultaneously induce severe thinning, cross-section distortion, and other defects. In addition, stretching can cause various failures initiations, some of which are non-visual and that may further affect product performance, for example, fatigue life, or energy absorption in crash management applications. Therefore, the stretching level applied in industrial forming process should be optimized to find a 'trade-off' between springback control, forming defects and product performance.

5.3. *Validation of analytical springback model*

The accuracy of the FM analytical model for springback assessment is studied by both physical experiments and FE simulations. In addition to the proposed FM analytical model, two alternative simplified approaches are also taken into account for comparison. These are briefly introduced as follows: *Reduced-FM model* is a simplified form based on the present FM model, which neglects the moment distribution beyond the bent portion while still considering the changes in cross-sectional geometry; *Classical model* is the most conventional and widely-used method for springback analysis in stretch bending [27,34], in which both the moment distribution outside the theoretically bent portion as well as the mass conservation effects are neglected. Unlike the FM and reduced-FM models, which use the true stress-true strain curve for calculation, the engineering stress–strain relationship is applied in the classical model.

Before assessment of the analytical models, the FE simulation accuracy for springback is evaluated. As shown in Fig. 19 (a), the FE simulated springback chord heights agree well with the experimental ones, as illustrated by a low average relative error of 2.38%. It also can be found that, except for the case with 4.15% stretching strain, the relative errors for different stretching levels are less than about 2.0%. Thus, the FE simulations presented herein provide good accuracy for springback prediction and can thus be used to evaluate mechanisms associated with the assumptions made in the FM analytical models along with the crucial deformation characteristics in stretching-controlled bending processes.

Fig. 19 (a) compares the springback chord heights obtained by

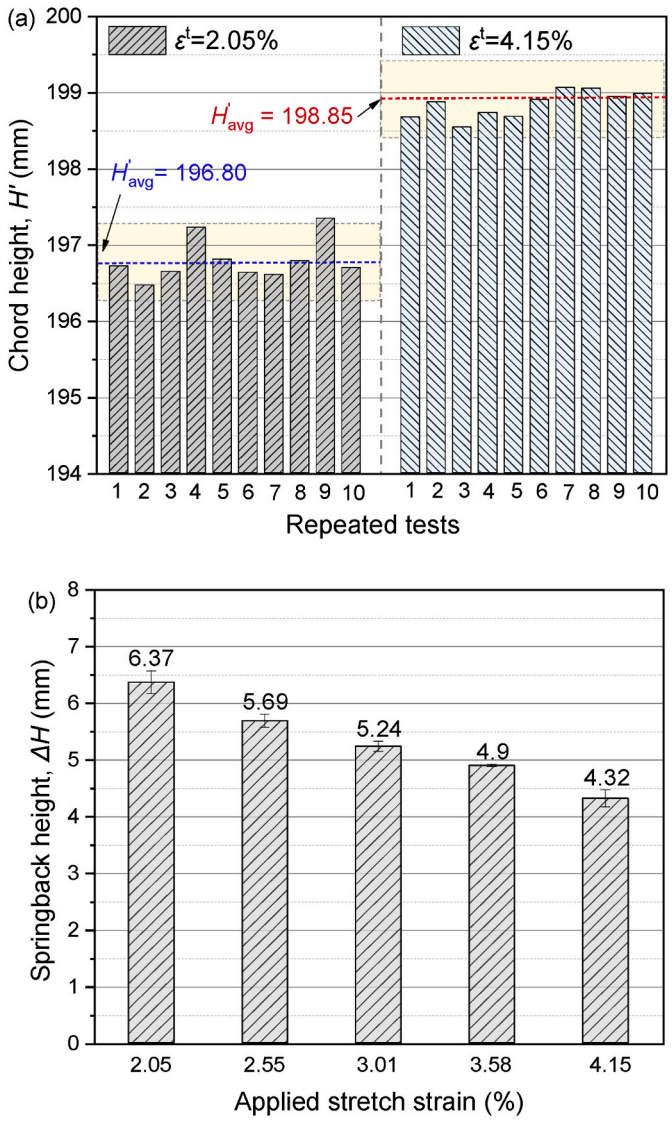

Fig. 18. Experimental results: (a) repeatability validation; (b) springback chord height under different stretch strain levels.

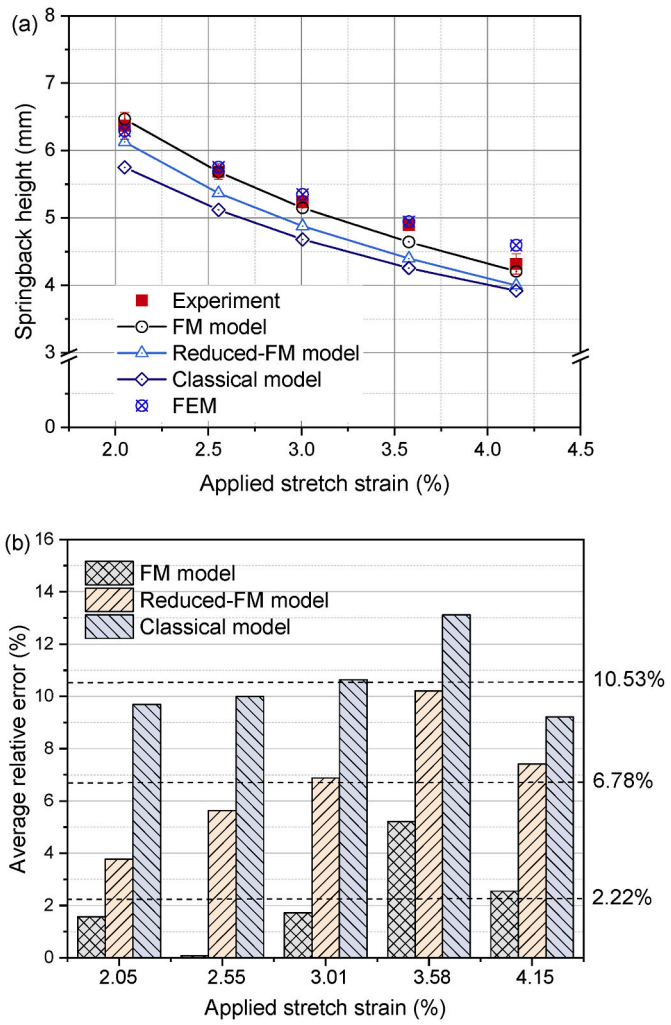

Fig. 19. Comparison among experiments, analytical predictions and FE simulations: (a) springback heights for different stretching levels; (b) error analysis of analytical models.

experiments, FE simulations and analytical calculations. It can be observed that the FM model does quite accurately predict springback chord height for a wide range of stretching strain levels. As shown in Fig. 19 (b), the average relative prediction error is less than about 2.22%, showing comparable capability for accurate springback assessment to the FE numerical method. When examining the analytical springback at different strain levels, the relative errors are around or less than the average error except for the case with 3.58% stretching strain with a relatively large error of about 5.21%. Comparing the prediction accuracy of the other two analytical methods, it can be found that the reduced-FM model, however, underestimates springback with an average relative error of 6.78%, while the classical model also underestimates springback but with a higher error of 10.53%. Overall, the FM model achieves a significant improvement for springback prediction compared to the reduced-FM model and the classical model.

Furthermore, the comparison between FM model and the other analytical models, this work indicates that the former, considering the internal moment distributed in the bending-stretching transition zones, can provide about 4.65% improvement of the prediction accuracy. This improvement is slightly more significant than the contribution made by the dimensional changes of cross-sectional members due to incompressibility upon plastic deformation. It should be noted that the springback chord height depends on the length of the straight portion and where the straight position is located relative to the reference measurement point location. In this study, as shown in Fig. 16 (b), the reference points for measuring the springback chord height are near the profile's ends, meaning that almost the entire profile is considered for springback analysis. In the experiments, the length of the straight portion of the target part is not sufficient long to ensure that the entire straight length is included in the transition portion. If the length of the straight portion is increased, the expected improvement of the accuracy of the FM model will increase, as compared to the reduced-FM and classical models since the contribution by the moment in the transition zone is neglected in the latter two models. In such a case, the FM model would expectedly provide improved springback assessment capability.

It is well-known that the analytically-based methods have more or less limitations when applied in practical problems. For the FM model proposed herein, due to the necessary assumptions employed, the main limitation is the applicability in forming of large-curvature (tight-radius bending) shapes. On one hand, the NL shifting in this model only depends on the applied stretching level assuming initially plane sections remain plane upon forming. For large-curvature bending, the assumption of a linear distribution of strain may create an error in the calculation of stress distribution across the profile depth, hence reducing the analytical accuracy of moment distribution and thus the springback assessment. Moreover, tight-radius bending can also induce severe

flange sagging during forming, which accordingly leads to the critical problems, for example, local distortions, local unloading affecting the moment and stress distributions, along with stiffness and springback. However, local flange sagging phenomena is beyond the mechanisms considered in the present model. In addition, several secondary aspects may also limit the applicability of the model. For example, the influence of loading path on springback is not modeled due to the total strain theory employed in the model. Also, the friction between the workpiece and forming dies is not considered, and the clamping-induced stresses and deformations are neglected.

Overall, even though several limitations do exist, the developed FM analytical model can still provide good capability for springback assessment in most kinematically-controlled stretch bending cases, since this type of bending processes is commonly used for forming relatively large-radius shapes. This means that the above-mentioned limitations are usually of minor importance in industrial practice.

5.4. Analysis of deformation characteristics

Using the FM analytical model combined with FE simulation, the deformation characteristics in the flexible stretch bending process of AA6082-T4 profiles are analyzed. Fig. 20 (a) shows the analytical strain distributions in the longitudinal direction of the innermost and outermost layers of the entire profile when formed at 2.05% stretching strain. It can be found that there is no MUS zone and EUS zone in the profile, since the length of the straight portion is too short. For the strain distribution predicted by the FM model, there are strain transition zones between UB and MUS/EUS zones, thus leading to the transition of strain gradient across the profile depth. For the results predicted by the classical model, however, the strain distributions change abruptly at the boundary between the bending portion and the straight portions, meaning that it theoretically does not fully obey the deformation theory of a continuum. As shown in Fig. 20 (c), the strain transition between the UB and the MUS/EUS zones also can be observed in the FE simulated

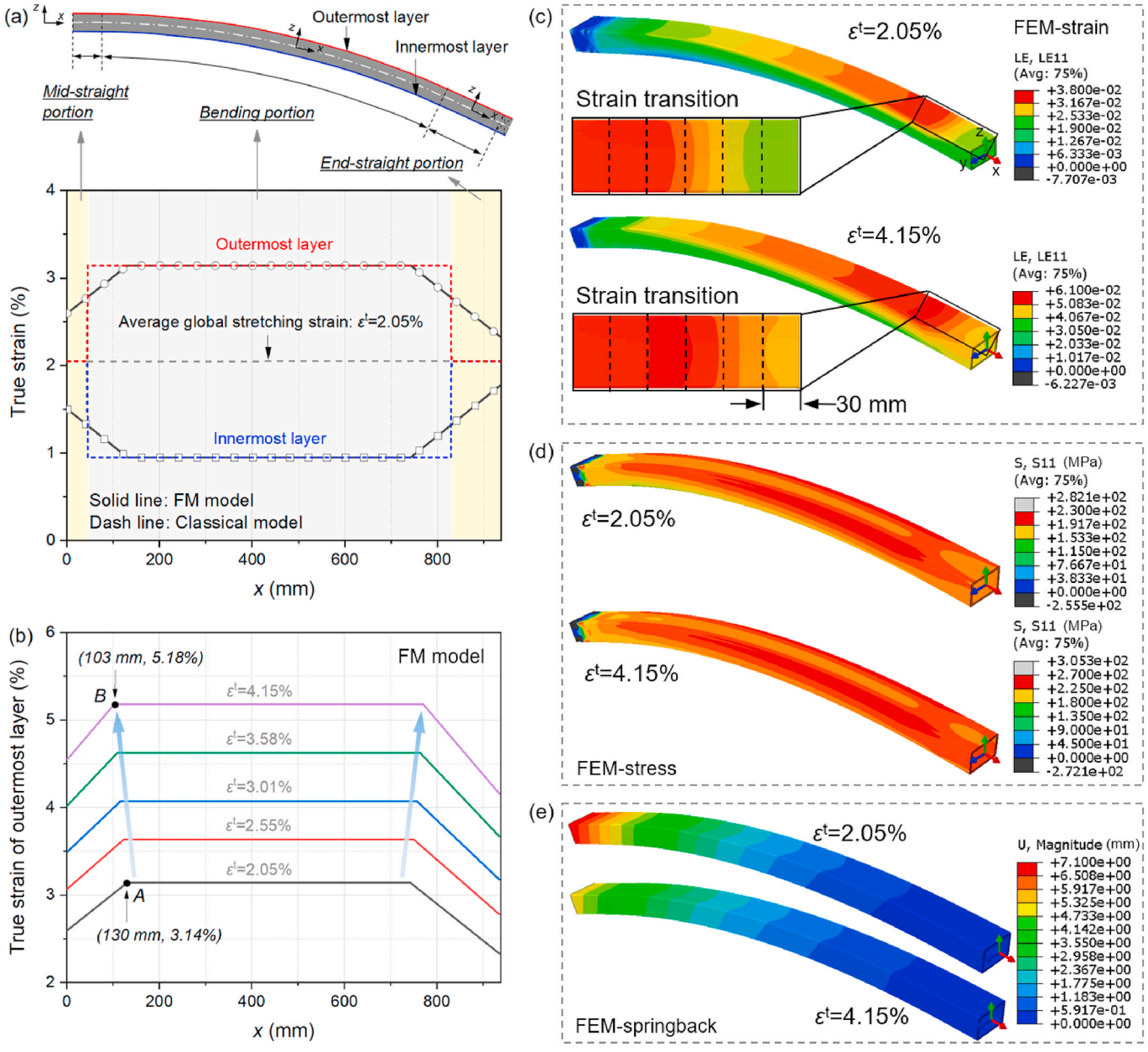

Fig. 20. Analysis of deformation behaviors of the formed profiles: (a) analytical strain distributions at 2.05% stretching; (b) analytical strain distribution within 2.05–4.15% stretching; (c) FE simulated strain distribution; (d) FE simulated stress distribution; (e) FE simulated springback distribution.

results. However, it should be noted that the FE simulated strain distribution along the longitudinal direction of the entire formed parts is nonuniform, and there is no such absolute uniform strain zone as described in the FM analytical model. Except for the transition zone near the mid-section ($x = 0$ mm), the FE model shows that the longitudinal strain gradually decreases from the area near the mid-section to the end ($x = 935$ mm) of the bent profile, which further results in such a stress distribution where the longitudinal stress slightly decreases from the middle to the end, as shown in Fig. 20 (d). When comparing the strain distribution predicted by the analytical method and the FE method, as illustrated in Fig. 20 (a) and (c), it is observed that the former predicts a strain of the outermost layer in the UB zone that reflects the average level of the FE simulated strain distribution in this zone. However, the deformation behaviors are more complex than those that can be described by the analytical models; for example, the effects of loading path, friction and local flange distortion (sagging) are not considered in the present analytical models. As shown in Fig. 20 (d), due to the slight sagging of the outer flange during forming, the stress near to the flange corner of the profile is higher than that in the middle, leading to local 'unloading' and a nonuniform distribution of stress (and strain) across the width of the external flange.

In addition, the strain distributions of the outermost layer under stretching strain levels of 2.05–4.15% are calculated by the FM analytical model to analyze the stretching-dependent evolution of the strain transition phenomenon. As shown in Fig. 20 (b), when the global stretching level is increased, the transition length is shortened (the UB zone is expanded) due to the reduced stress gradient across the profile depth in the UB zone. Furthermore, the stretching-dependent evolution of strain transition can also be verified in the FE simulation. As demonstrated in Fig. 20 (c), taking the transition zone near the mid-section for a detailed analysis, it can be clearly seen that the strain transition phenomenon at the outermost layer under the lower stretching level (2.05%) is longer than that under a higher stretching level (4.15%). Comparing the middle transition lengths obtained by the FM analytical model (Fig. 20 (b)) and the FE simulation (Fig. 20 (c)), it can be found that analytical results under both lower and higher stretching levels agree well with the FE simulated ones; i.e., about 100 mm and 130 mm under 2.15% and 4.15% stretching strains, respectively. Thus, the FE results support important assumptions made in FM analytical model. The stretching-dependent evolution of strain transition can make a difference in the distributions of stress and moment of the entire formed part, thus affecting the global springback, as illustrated in Fig. 20 (e). Here mainly analyzes the strain transition behavior in the bending cases with stretching strains of 2.05–4.15%. Based on the governing equation of strain transition proposed in Section 3.3.2, if the stretching level upon forming is continuously increased, the stress difference between UB zone and MUT/EUT zones (equivalent to the stress gradient across the profile depth) is reduced, and the strain transition area will be reduced accordingly.

Furthermore, the moment distribution in the longitudinal direction of the entire formed part is analyzed, as shown in Fig. 21. The moment distribution predicted by the FM model consists of a uniform distribution in the UB zone and two reduced transitions from the UB zone to the mid-section and the end of the profile, due to the above-described assumptions. In the analytical calculation by the classical model, the moment is only uniformly distributed in the bending portion. Comparing the moment distribution of the UB zone under the stretching levels of 2.05% and 4.15%, it can be found that the moment obtained by the FM model is slightly higher than that obtained by the classical model under 2.05% stretching strain, while the classical model presents a little higher moment under 4.15% stretching. It should be noted that the moment difference calculated by the FM model and the classical model are as small (about 6 N·m). However, it can be found from the bending case with 2.05% stretching that the moments at $x = 0$ mm and $x = 935$ mm can still reach about 72 and 36 N·m, respectively, which is much larger than the moment difference of the UB zone calculated by the two

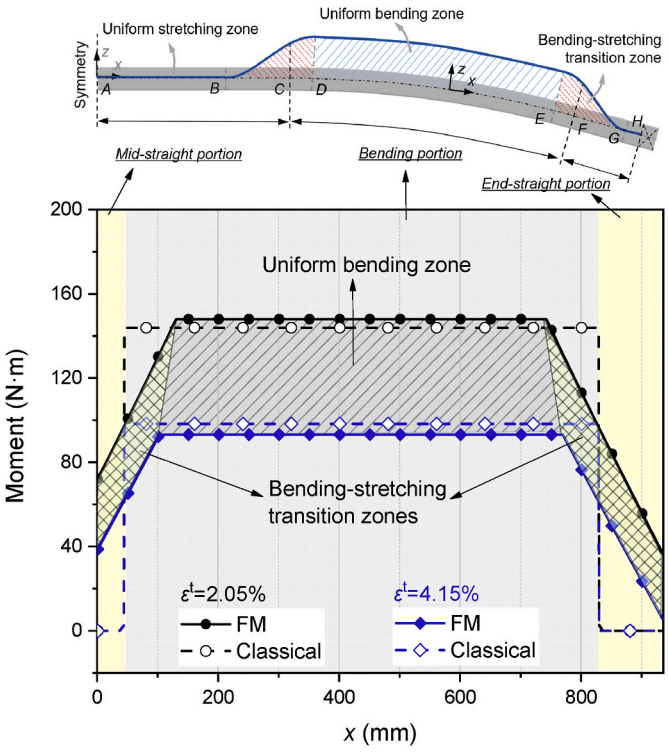

Fig. 21. Moment distribution in the formed profiles.

methods. Thus, the moment distributed in the transition zones can make a significant contribution to the global springback, given that the entire part is under heavy stretching. It also can be observed from Fig. 21 that, when high stretching level is applied, the transition length is shortened, thus reducing the effect of the strain transition on the global springback. Moreover, with increased stretching level, the second moment of inertia trends to decrease due to changes of the sectional dimensions (thickness, width and depth). This leads to more accurate prediction of springback with the FM model than with the classical model.

6. Conclusions and outlook

Springback is a major problem affecting the dimensional accuracy of formed products, process flexibility, manufacturing cost, and productivity (OEE). Effective prediction of springback is a challenge due to its crucial sensitivity to upstream and in-process parameters. In this work, an analytical framework for accurate springback assessment in stretching-controlled, flexible bending process is developed, aiming to make springback knowledge more explicit, generic and reuseable. The main conclusions of this work can be summarized as follows:

- A new flexible, 3D rotary stretch bending method for fabrication of complex-shape profiles is presented, and a full-scale machine is designed and built. The innovative machine design is based on adding the number of rotational/translational axes in conjunction with a flexible tooling design concept, which enables the manufacture of complex and flexible geometrical configurations with low tool investments.
- A Full Moment (FM) analytical framework for springback assessment is developed. In this model, the internal moment distribution along the entire formed part upon stretch bending is modeled. This strategy enables the contribution of the plastic moment distribution beyond the theoretically bent portions can be considered in the global springback analysis. Moreover, the influential parameters of material, geometry and process are comprehensively modeled. This analytical model improves the applicability and capability for

evaluating springback of complex part configurations in kinematically-controlled bending processes, while enabling exploration of springback characteristics and compensation strategies.

- Carefully designed experiments with applying different stretching levels prove that the new flexible bending process provides superior capability for controlling springback, thus improving the dimensional accuracy of products. Doubling the stretching strain from about 2% to 4%, the springback chord height can be reduced by one third, which significantly improves the process capability (C_p).
- A comparative study between experiments, numerical simulations and analytical calculations shows that the FM analytical modeling strategy provides accurate assessment of springback in stretch bending cases undergoing a wide range of stretching levels. The main limitations of the FM model include neglection of mechanisms related to tight-radius bending, friction, local distortion, and clamping. Using the analytical models combined with the FE simulation, the crucial deformation characteristics, including the stretching-dependent evolution of strain transition, important to the understanding of the process are revealed and interpreted.

Overall, the present analytical model provides an effective means to enhance the understanding of springback mechanisms, thus creating a basis for making such knowledge more explicit, generic and reuseable in industrial practice. Although the model and experimental validation presented herein concerns manual 'feedback prediction' of springback in 2D, the strategy can be extended to the forming of 3D shapes with automated, closed-loop feedback control of springback as part of the machine control system. However, the latter would require successful integration of sensor and vision technologies that provide acceptable accuracy for closed-loop feedback to the control system of the bending machine and tools, along with the demonstration of operational robustness in a manufacturing plant environment.

Author statement

Jun Ma: Conceptualization, Methodology, Investigation, Formal analysis, Writing - original draft, Writing - review and editing. Torgeir Welo: Conceptualization, Methodology, Investigation, Supervision, Writing - review and editing.

Declaration of competing interest

The authors declare that they have no known competing financial interests or personal relationships that could have appeared to influence the work reported in this paper.

Acknowledgements

The authors gratefully acknowledge the financial support from Norwegian University of Science and Technology (NTNU), NTNU Aluminium Product Innovation Center (NAPIC) and the KPN Project VALUE (No. 267768) sponsored by The Research Council of Norway, Hydro and Alcoa. In addition, the authors would like to thank Dr. J. Blindheim and Mr. T. Ha at NTNU for the help with machine calibration, experiments and discussions.

References

[1] S. Rosenthal, F. Maaß, M. Kamaliev, M. Hahn, S. Gies, A.E. Tekkaya, Lightweight in automotive components by forming technology, Automot. Innov. 3 (2020) 195–209.
[2] J. Cao, M. Banu, Opportunities and challenges in metal forming for lightweighting: review and future work, J. Manuf. Sci. Eng. 142 (2020) 1–24.
[3] T. Welo, G. Ringen, J. Ma, An overview and evaluation of alternative forming processes for complex aluminium products, Procedia Manuf 48 (2020) 82–89.
[4] J. Hirsch, Recent development in aluminium for automotive applications, Trans. Nonferrous Metals Soc. China 24 (2014) 1995–2002.
[5] F. Vollertsen, A. Sprenger, J. Kraus, H. Arnet, Extrusion, channel, and profile bending: a review, J. Mater. Process. Technol. 87 (1999) 1–27.
[6] T. Welo, J. Ma, J. Blindheim, T. Ha, G. Ringen, Flexible 3D stretch bending of aluminium alloy profiles: an experimental and numerical study, Procedia Eng 50 (2020) 37–44.
[7] H. Li, H. Yang, M. Zhan, Z.C. Sun, R.J. Gu, Role of mandrel in NC precision bending process of thin-walled tube, Int. J. Mach. Tool Manufact. 47 (7) (2007) 1164–1175.
[8] A. Ghiotti, E. Simonetto, S. Bruschi, P.F. Bariani, Springback measurement in three roll push bending process of hollow structural sections, CIRP Ann. - Manuf. Technol. 66 (2017) 289–292.
[9] S. Chatti, M. Hermes, A.E. Tekkaya, M. Kleiner, The new TSS bending process: 3D bending of profiles with arbitrary cross-sections, CIRP Ann. - Manuf. Technol. 59 (2010) 315–318.
[10] K.B. Müller, Bending of extruded profiles during extrusion process, Int. J. Mach. Tool Manufact. 46 (2006) 1238–1242.
[11] W. Zhou, J. Lin, T.A. Dean, L. Wang, Feasibility studies of a novel extrusion process for curved profiles: experimentation and modelling, Int. J. Mach. Tool Manufact. 126 (2018) 27–43.
[12] X. Guo, H. Xiong, H. Li, Y. Xu, Z. Ma, A.A. El-aty, Y. Ma, K. Jin, Forming characteristics of tube free-bending with small bending radii based on a new spherical connection, Int. J. Mach. Tool Manufact. 133 (2018) 72–84.
[13] C. Lin, G. Chu, L. Sun, G. Chen, P. Liu, W. Sun, Radial hydro-forging bending: a novel method to reduce the springback of AHSS tubular component, Int. J. Mach. Tool Manufact. (2020) 103650. In press.
[14] J. Ma, T. Ha, J. Blindheim, T. Welo, G. Ringen, H. Li, Exploring the influence of pre/post-aging on springback in Al-Mg-Si alloy tube bending, Procedia Manuf 47 (2020) 774–780.
[15] R.H. Wagoner, H. Lim, M.G. Lee, Advanced issues in springback, Int. J. Plast. 45 (2013) 3–20.
[16] J.M. Allwood, S.R. Duncan, J. Cao, P. Groche, G. Hirt, B. Kinsey, T. Kuboki, M. Liewald, A. Sterzing, A.E. Tekkaya, Closed-loop control of product properties in metal forming, CIRP Ann. - Manuf. Technol. 65 (2016) 573–596.
[17] D.Y. Yang, M. Bambach, J. Cao, J.R. Duflou, P. Groche, T. Kuboki, A. Sterzing, A. E. Tekkaya, C.W. Lee, Flexibility in metal forming, CIRP Ann. - Manuf. Technol. 67 (2018) 743–765.
[18] H. Li, M.W. Fu, Deformation-Based Processing of Materials: Behavior, Performance, Modeling, and Control, Elsevier, 2019.
[19] R. Zhai, X. Ding, S. Yu, C. Wang, Stretch bending and springback of profile in the loading method of prebending and tension, Int. J. Mech. Sci. 144 (2018) 746–764.
[20] J.C. Liang, S. Gao, F. Teng, P.Z. Yu, X.J. Song, Flexible 3D stretch-bending technology for aluminium profile, Int. J. Adv. Manuf. Technol. 71 (2014) 1939–1947.
[21] Y. Zhou, P. Li, M. Li, L. Wang, Application and correction of L-shaped thin-wall aluminium in flexible-bending processing, Int. J. Adv. Manuf. Technol. 92 (2017) 981–988.
[22] Y. Li, Z. Shi, Q. Rong, W. Zhou, J. Lin, Effect of pin arrangement on formed shape with sparse multi-point flexible tool for creep age forming, Int. J. Mach. Tool Manufact. 140 (2019) 48–61.
[23] M.G. Lee, J.H. Kim, K. Chung, S.J. Kim, R.H. Wagoner, H.Y. Kim, Analytical springback model for lightweight hexagonal close-packed sheet metal, Int. J. Plast. 25 (2010) 399–419.
[24] H. Li, J. Ma, B.Y. Liu, R.J. Gu, G.J. Li, An insight into neutral layer shifting in tube bending, Int. J. Mach. Tool Manufact. 126 (2018) 51–70.
[25] A.E. Tekkaya, P.O. Bouchardb, S. Bruschi, C.C. Tasand, Damage in metal forming, CIRP Ann. - Manuf. Technol. 35 (2020) 1–24.
[26] T.X. Yu, W. Johnson, Influence of axial force on the elasto-plasticbending and springback of a beam, J. Mech. Work. Technol. 6 (1982) 5–21.
[27] M. Geiger, A. Sprenger, Controlled bending of aluminium extrusions, CIRP Ann. - Manuf. Technol. 47 (1998) 197–202.
[28] A.A. El-Domiaty, Stretch forming of beams of nonuniform section, J. Mater. Process. Technol. 22 (1999) 21–28.
[29] A.A. El-Domiaty, A.A. Elsharkawy, Stretch-bending analysis of U-section beams, Int. J. Mach. Tool Manufact. 38 (1998) 75–95.
[30] A.A. El-Domiaty, A.A. Elsharkawy, Determination of stretch-bendability limits and springback for T-section beams, J. Mater. Process. Technol. 110 (2001) 265–276.
[31] J. Zhao, J. Yin, R. Ma, L. Ma, Springback equation of small curvature plane bending, Sci. China Technol. Sci. 54 (2011) 2386–2396.
[32] J. Zhao, R. Zhai, Z. Qian, R. Ma, A study on springback of profile plane stretch-bending in the loading method of pretension and moment, Int. J. Mech. Sci. 75 (2013) 45–54.
[33] H. Zhu, K.A. Stelson, Modeling and closed-loop control of stretch bending of aluminium rectangular tubes, J. Manuf. Sci. Eng. Trans. ASME 125 (2003) 113–119.

[34] T. Liu, Y. Wang, J. Wu, X. Xia, J. Wang, W. Wang, S. Wang, Springback analysis of Z & T-section 2196-T8511 and 2099-T83 Al-Li alloys extrusions in displacement controlled cold stretch bending, J. Mater. Process. Technol. 225 (2015) 295–309.
[35] J.E. Miller, S. Kyriakides, A.H. Bastard, On bend-stretch forming of aluminium extruded tubes - I: Experiments, Int. J. Mech. Sci. 43 (2001) 1283–1317.
[36] J.E. Miller, S. Kyriakides, Three-dimensional effects of the bend – stretch forming of aluminium tubes, Int. J. Mech. Sci. 45 (2003) 115–140.
[37] T. Welo, B. Granly, A new adaptive bending method using closed loop feedback control, Trans. Nonferrous Metals Soc. China 20 (2010) 2111–2117.
[38] T. Welo, Intelligent manufacturing systems: controlling elastic springback in bending, IFIP Adv. Inf. Commun. Technol. 397 (2012) 460–466.
[39] G. Grzancic, C. Löbbe, N. Ben Khalifa, A.E. Tekkaya, Analytical prediction of wall thickness reduction and forming forces during the radial indentation process in Incremental Profile Forming, J. Mater. Process. Technol. 267 (2019) 68–79.
[40] T.X. Yu, L.C. Zhang, Plastic Bending: Theory and Applications, World Scientific, Singapore, 1996.
[41] J.A. Garza-Reyes, S. Eldridge, K.D. Barber, H. Soriano-Meier, Overall equipment effectiveness (OEE) and process capability (PC) measures: a relationship analysis, Int. J. Qual. Reliab. Manag. 27 (2010) 48–62.